

1 **Anthropogenic activities significantly increase annual**
2 **greenhouse gas (GHG) fluxes from temperate headwater**
3 **streams in Germany**

4 **Authors:** Ricky Mwangada Mwanake¹; Gretchen Maria Gettel^{2,7}, Elizabeth Gachibu
5 Wangari¹, Clarissa Glaser⁵, Tobias Houska⁴, Lutz Breuer^{4,6}, Klaus Butterbach-Bahl^{1,3}, Ralf
6 Kiese¹

7

8 ¹Karlsruhe Institute of Technology, Institute for Meteorology and Climate Research, Atmospheric
9 Environmental Research (IMK-IFU), Kreuzeckbahnstrasse 19, Garmisch-Partenkirchen 82467, Germany

10 ²IHE-Delft Institute for Water Education, Westvest 7 2611 AX Delft the Netherlands

11 ³Pioneer Center Land-CRAFT, Department of Agroecology, University of Aarhus, Denmark

12 ⁴Institute for Landscape Ecology and Resources Management (ILR), Research Centre for BioSystems, land use /
13 land cover and Nutrition (iFZ), Justus Liebig University Giessen, Giessen, 35392, Germany

14 ⁵Center for Applied Geoscience, University of Tübingen, Tübingen, Germany

15 ⁶Centre for International Development and Environmental Research (ZEU), Justus Liebig University Giessen,
16 Senckenbergstrasse 3, 35390 Giessen, Germany

17 ⁷Department of Ecoscience, Lake Ecology, Aarhus University, Denmark

18

19 *Correspondence to* Ralf Kiese (ralf.kiese@kit.edu)

20 **Abstract**

21 Anthropogenic activities increase the contributions of inland-waters to global greenhouse gas (GHG;
22 CO₂, CH₄, and N₂O) budgets, yet the mechanisms driving these increases are still not well constrained. In this
23 study, we quantified year-long GHG concentrations, fluxes, and water physico-chemical variables from 28 sites
24 contrasted by land use across five headwater catchments in Germany. Based on linear mixed effects models, we
25 showed that land use was more significant than seasonality in controlling the intra-annual variability of the
26 GHGs. Streams in agricultural-dominated catchments or with wastewater inflows had up to 10 times higher daily
27 CO₂, CH₄, and N₂O emissions and were also more temporally variable (CV > 55%) than forested streams. Our
28 findings also suggested that nutrient, labile-carbon, and dissolved GHG inputs from the agricultural and
29 settlement areas may have supported these hotspots and hot-moments of fluvial GHG emissions. Overall, the
30 annual emission from anthropogenic-influenced streams in CO₂-equivalents was up to 20 times higher (~71 kg
31 CO₂ m⁻² yr⁻¹) than from natural streams (~3 kg CO₂ m⁻² yr⁻¹), with CO₂ accounting for up to 81 % of these annual
32 emissions, while N₂O and CH₄ accounted for up to 18 and 7 %, respectively. The positive influence of
33 anthropogenic activities on fluvial GHG emissions also resulted in a breakdown of the expected declining trends
34 of fluvial GHG emissions with stream size. Therefore, future studies should focus on anthropogenically
35 perturbed streams, as their GHG emissions are much more variable in space and time and can potentially
36 introduce the largest uncertainties to fluvial GHG estimates.

37 **1 Introduction**

38 Streams and rivers cover only a small fraction of the earth's land surface (0.4%; Allen et al., 2018), yet
39 they are significant contributors to global greenhouse (CO₂, CH₄, and N₂O) budgets, emitting approximately 7.6
40 (6.1–9.1) Pg-CO₂ equivalent into the atmosphere per year (Li et al., 2021). Headwater streams are hotspots for
41 GHG emissions within fluvial ecosystems due to their large surface area to volume ratio compared to larger
42 rivers, allowing for close connectivity with GHG sources (Hotchkiss et al., 2015; Turner et al., 2016). Several
43 biogeochemical processes are responsible for GHG production and consumption within headwater ecosystems.
44 Biogenic CO₂ production is mainly attributed to the respiration of organic matter (Battin et al., 2008). Production
45 of CH₄ occurs through methanogenesis, with carbon dioxide and acetic acid as substrates under anaerobic
46 conditions (Stanley et al., 2016). Methane consumption is also possible through methanotrophy in oxygen-rich
47 stream waters, producing CO₂ (Shelley et al., 2014). N₂O is mainly a byproduct in nitrification (under aerobic
48 conditions) or an intermediate product in denitrification (under anaerobic conditions), but it can also be reduced
49 to N₂ in organic-rich and nitrate-poor ecosystems (Quick et al., 2019). Apart from instream biogeochemical
50 production, GHG concentrations in headwater streams may also come from external sources such as
51 groundwater and terrestrial soils (e.g., Borges et al., 2015; Hotchkiss et al., 2015). These external sources are
52 generally dominant during periods of heavy precipitation when the hydrological connectivity between the
53 streams and their surrounding terrestrial landscape and groundwater is activated. Yet, partitioning the sources of
54 these GHGs between in-situ production and external sources remains a challenge to aquatic scientists, as their
55 contributions are mainly compounded and also vary widely depending on discharge conditions and the
56 surrounding land use (e.g., Aho & Raymond, 2019; Borges et al., 2019; Mwanake et al., 2022).

57 Within headwaters, anthropogenic practices such as fertilizer application and construction of drainage
58 ditches to allow agricultural use of former wetlands alter the rates of *instream* GHG production and their external
59 sources, thereby influencing their spatial-temporal dynamics (Peacock et al., 2021; Wallin et al., 2020; Mwanake
60 et al., 2019). Elevated hydrological inputs of dissolved GHGs, nutrients, and labile carbon to streams from
61 fertilized croplands have been shown to increase their N₂O (e.g., Beaulieu et al., 2009; Mwanake et al., 2019),
62 CO₂ (e.g., Bodmer et al., 2016; Borges et al., 2018), and CH₄ fluxes (e.g., Deirmendjian et al., 2019; Mwanake et
63 al., 2022), by favoring *instream* GHG production processes and also ensuring steady supplies in periods of low
64 in-situ biogeochemical production. While such trends in agricultural streams show similarities across different
65 catchment locations, GHG emissions from streams in predominantly forested catchments with minor influences
66 from croplands and wetlands show more diverse patterns. Some studies indicated that forest streams are hotspots
67 for GHG fluxes (e.g., Wallin et al., 2018; Audet et al., 2019; Herreid et al., 2021), while others found the
68 opposite with much lower fluxes in forests as compared to other land uses (e.g., Bodmer et al., 2016; Mwanake
69 et al., 2022). Besides draining CH₄ and CO₂-rich terrestrial soils, drainage ditches are characterized by short
70 water residence times, high organic loads, and highly variable O₂ levels, which can simultaneously support
71 vigorous CH₄ and CO₂ production and, subsequently, higher fluxes. For example, in a recent meta-analysis,
72 ditches, and canals accounted for up to 3% of the global anthropogenic CH₄ emissions (Peacock et al., 2021).
73 Yet, studies on them are scarce, and thus the main factors making them hotspots of carbon fluxes are still not
74 well-constrained.

75 In fluvial ecosystems within settlement areas, point-source inflows of wastewater effluents have also
76 been reported to alter natural GHG trends along the river continuum (Park et al., 2018). The wastewater effluent
77 is either substrate-rich, favoring insitu GHG production, or GHG-rich, resulting in high riverine GHG emissions
78 downstream of the inflow point (e.g., Marescaux et al., 2018; Begum et al., 2021; Zhang et al., 2021; Wang et
79 al., 2022). For example, in a study of urban-impacted rivers in the Seine basin in France, Marescaux et al. (2018)
80 found elevated CO₂, CH₄, and N₂O concentrations and fluxes downstream of wastewater inflows, which
81 disproportionately contributed up to 52 % of the basin-wide annual GHG fluxes. Similar findings were also
82 found in urban-impacted rivers in China, where their GHG emissions were up to 14 times higher than those in
83 other land uses (Zhang et al., 2021). Yet, studies on GHG emissions from urban-impacted fluvial ecosystems are
84 still scarce, and therefore their contributions to riverine annual GHG budgets are not well constrained. Moreover,
85 little is known about the cumulative effects of diffuse and point pollution sources on the magnitude of riverine
86 GHG fluxes and whether the diffuse pollution sources exert longer-lasting controls on their fluxes than the point
87 sources.

88 Under temperate climatic conditions, pronounced seasonality regulates the availability of nutrients and,
89 to some extent, the O₂ in lotic ecosystems, which are both key factors driving *instream* GHG production and gas
90 exchange rates (Borges et al., 2018; Rocher-Ros et al., 2019; Herreid et al., 2021; Aho et al., 2022). Cold winter
91 periods are generally characterized by low *instream* carbon and nitrogen processing, which results in nutrient
92 accumulation (e.g., Herreid et al., 2021). In contrast, high *instream* C and N processing are characteristic of
93 warm summer periods (e.g., Borges et al., 2018; Aho et al., 2021, 2022). Seasonality in precipitation regulates
94 discharge, whereby heavy precipitation events or snowmelt during spring result in high discharge events. At the
95 same time, dry summers and winter periods are often characterized by lower discharge (e.g., Aho et al., 2022).
96 Discharge determines the water residence times in streams, which controls the rates of *instream* C and N

97 processing. Previous studies have shown that low discharge periods with longer water residence times favor
98 instream GHG production processes (e.g., Borges et al., 2018; Mwanake et al., 2022). In comparison, high
99 discharge periods with shorter water residence times are unfavorable to *instream* C and N cycling, resulting in
100 the dominance of externally sourced GHGs from upstream terrestrial sources depending on the surrounding land
101 use. For example, studies have found that during high discharge periods, streams draining wetlands show peak
102 CO₂ and CH₄ concentrations (e.g., Aho et al., 2019; Borges et al., 2019), and pronounced N₂O concentrations are
103 found in streams of cropland-dominated catchments (e.g., Mwanake et al., 2022).

104 The dynamic interactions between seasonality and land use discussed above indicate that less frequent
105 measurements of riverine GHG concentrations and fluxes may fail to capture periods of elevated fluvial
106 emissions at spatially hotspot areas, resulting in an underestimation of the annual emissions. Yet, only a handful
107 of studies in temperate streams have assessed the seasonal dynamics of GHG fluxes at sampling points with
108 contrasting land uses (e.g., Marescaux et al., 2018; Borges et al., 2018; Herreid et al., 2021; Galantini et al.,
109 2021), resulting in uncertainties in the mechanisms that drive either hot periods or hotspots of fluvial GHG
110 fluxes. As climate change causes more extreme discharge conditions and as agricultural intensification and
111 settlement areas continue to increase (Winkler et al., 2021), more studies that cover a wide array of land uses,
112 discharge, and temperature conditions are needed to allow developing better mechanistic understanding of their
113 effects on fluvial GHG dynamics by unraveling synergistic or antagonistic relationships amongst them. These
114 increased process understanding will form the basis of future mechanistic modeling approaches, which are
115 essential to predict better how fluvial GHG emissions will respond to future climate and land use changes (Battin
116 et al., 2023).

117 The main objective of this study was to assess the seasonality-land use relationships of water physico-
118 chemical variables and GHG concentration and fluxes by comparing temperate lotic ecosystems of forests and
119 wetlands with those from more human-influenced agricultural and settlement catchments. To do so, we
120 conducted at least tri-weekly measurements covering a full year of observations and mainly focused on
121 headwater streams (stream orders 1–6), which despite being hotspots of fluvial emissions, remain currently
122 underrepresented in global GHG datasets (Drake et al., 2018; Li et al., 2021). We hypothesize that catchment
123 land use is the most critical control for stream GHG concentration and fluxes, with higher seasonal variability in
124 human-influenced ecosystems than in natural ones. Moreover, we hypothesized that drainage ditches and
125 headwater streams with wastewater inflow within agricultural and settlement areas are hotspots for GHG
126 emissions, driven by direct dissolved GHG inputs or substrate inputs that favor *in situ* GHG production.

127 2 Materials and methods

128 2.1 Study areas and sampling design

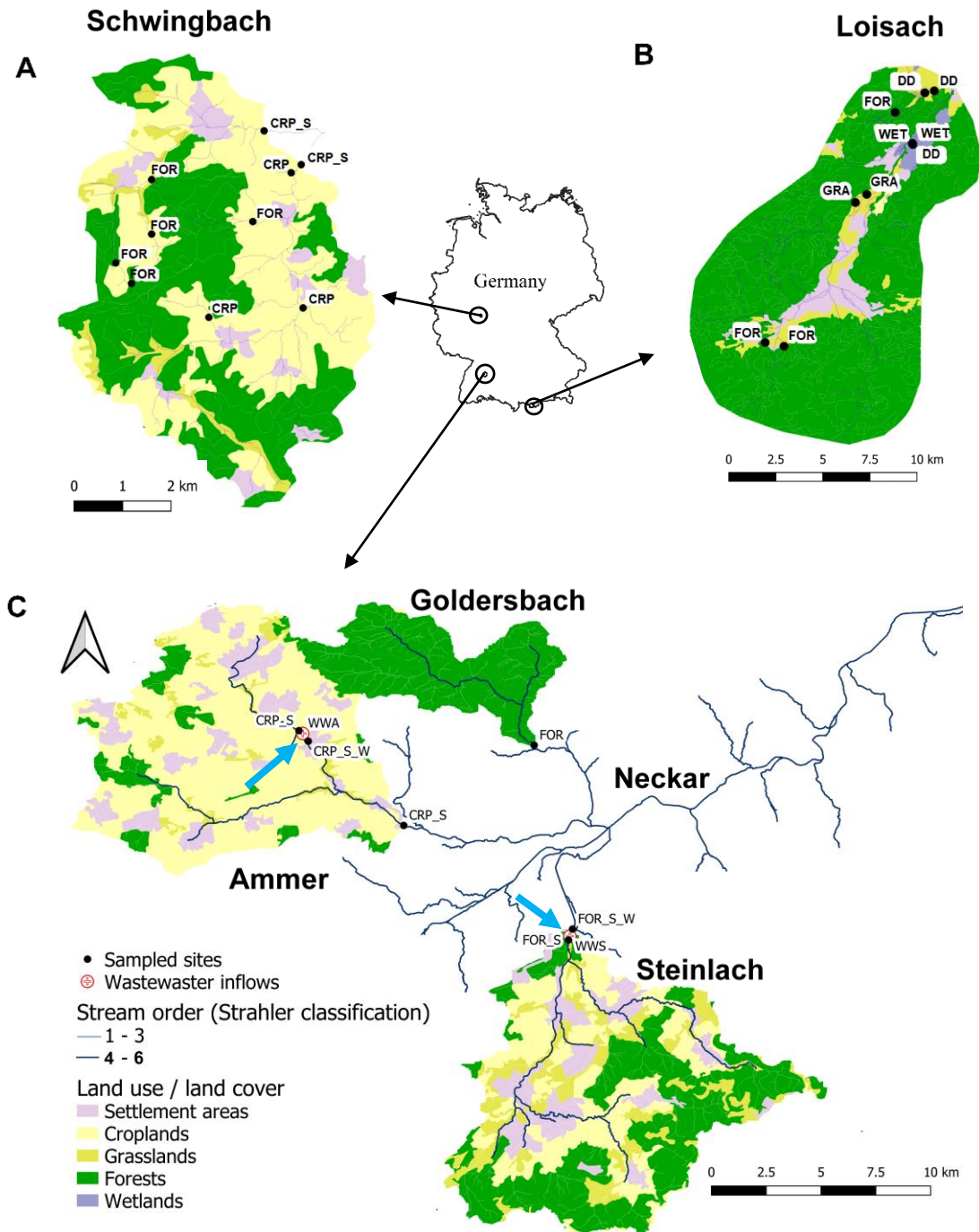
129 Five headwater catchments in central (Schwingbach), southeast (Loisach), and southwest (Ammer,
130 Goldersbach, and Steinlach) Germany were investigated in this study. The catchments covered a wide range of
131 fluvial ecosystems with different stream orders and land use characteristics (Table 1; Fig. 1). The catchment
132 boundaries for each site were determined based on the most downstream sampling location within each
133 catchment (Fig. 1). Elevation of the Schwingbach catchment (54 km²), located in the central-German state of

134 Hessen, ranges from 176–480 m above sea level (a.s.l). The catchment has a mixed land use of ~41 % mixed
135 forests, 46% croplands, 8 % settlement areas, and 5 % pasturelands (Wangari et al., 2022) (Fig. 1A). The climate
136 is warm and temperate (Cfb, Köppen climate classification), with an annual rainfall of 742 mm (monthly mean
137 min: 51 mm, monthly mean max: 72 mm) (1999–2019) and a mean annual temperature of 9.8 °C (monthly mean
138 min: 1.3 °C, monthly mean max: 18.8 °C) (1991–2021) (Climate-data.org, [https://en.climate-](https://en.climate-data.org/europe/germany/hesse/giessen-151/)
139 [data.org/europe/germany/hesse/giessen-151/](https://en.climate-data.org/europe/germany/hesse/giessen-151/)).

140 The Upper Loisach catchment (467 km², outlet Eschenlohe town) is located in the mountainous region
141 of the Bavarian Alps, Germany. The catchment is characterized by a pronounced relief and steep slopes, with
142 elevations ranging from 616–2,963 m a.s.l. Land use in the catchment comprises coniferous and deciduous
143 forests interspersed with natural grasslands and rocky surfaces on the mountain slopes (78%). At the valley
144 bottom, the land use is mainly settlement areas (9%), managed grasslands (8%), and wetlands (5%) (Fig. 1B).
145 The climate is cold and temperate (Dfb, Köppen climate classification), with annual precipitation of 1,693 mm
146 (monthly mean min: 87 mm, monthly mean max: 207 mm) (1999–2019) and mean annual temperature of 3.8 °C
147 (monthly mean min: -6.6 °C, monthly mean max: 13.1 °C) (1991–2021) (Climate-data.org, [https://en.climate-](https://en.climate-data.org/europe/germany/free-state-of-bavaria/garmisch-partenkirchen-8762/)
148 [data.org/europe/germany/free-state-of-bavaria/garmisch-partenkirchen-8762/](https://en.climate-data.org/europe/germany/free-state-of-bavaria/garmisch-partenkirchen-8762/)).

149 The other three catchments are sub-catchments of the Neckar river (Fig. 1C). The Goldersbach (116
150 km²), a tributary of the main Ammer stream, is a forested catchment (95%), with elevations ranging from 366–
151 583 m a.s.l. The Steinlach catchment (513 km²) is also dominated by forests (74%), with agricultural lands
152 (croplands and grasslands) and settlement areas occupying 21% and 5% of the landscape, respectively. The
153 elevation range of the hilly area is 321–878 m a.s.l (Fig. 1C). The Ammer catchment (304 km², outlet
154 Pfäffingen) is dominated by agricultural lands (80%), with 11% forests and 9% settlement areas (Fig. 1C). It has
155 moderate slopes with an elevation ranging from 319–610 m a.s.l. The Ammer stream is a gaining stream fed by
156 an extensive groundwater karst system and has significant discharge levels even during the driest periods of the
157 year (Glaser et al., 2020). The climate is warm and temperate (Cfb, Köppen climate classification), with a mean
158 annual rainfall of 923 mm (monthly mean min: 63 mm, monthly mean max: 98 mm) (1999–2019) and a mean
159 annual temperature of 9.3 °C (monthly mean min: 0.2 °C, monthly mean max: 18.6 °C) (1991–2021) (Climate-
160 [data.org, https://en.climate-data.org/europe/germany/baden-wuerttemberg/tuebingen-22712/](https://en.climate-data.org/europe/germany/baden-wuerttemberg/tuebingen-22712/)).

161 Across the five catchments, a total of 28 sites at headwater streams (N=23, orders 1–6, defined after
162 Strahler, 1952), drainage ditches (N=3), and wastewater outflows (N=2, Text A1) were sampled every 2–3 weeks
163 for an entire year (Table 1, Fig. 1). The Schwingbach and Loisach catchments were sampled from June 2020 to
164 June 2021 while the Goldersbach, Ammer, and Steinlach catchments, were sampled from April 2021 to April
165 2022.



166

167 Fig. 1: Land cover maps of the (A) Schwingbach, (B) Loisach, and (C) Neckar sub-catchments (Goldersbach,
 168 Ammer, and Steinlach) derived from the Corine Land Cover 2018 inventory with a 25 ha spatial resolution
 169 (<https://land.copernicus.eu/pan-european/corine-land-cover/clc2018?tab=mapview>). Black dots with labels
 170 (abbreviations explained in Table 1) represent sampled headwater streams and drainage ditch sampling points.
 171 Wastewater inflows sampled are indicated by blue arrows on the maps. Drainage ditches in the Loisach
 172 catchment were dug in the 1930s to 1960s to lower water levels to improve grassland productivity in areas
 173 formerly occupied by wetlands.

174 2.2 Sub-catchment delineation and land use classification

175 Sub-catchments for each sampling point in the Loisach, Goldersbach, Steinlach, Ammer, and
176 Schwingbach catchments were delineated in QGIS from a Digital Elevation Model (DEM) (EU-DEM v1.1) with
177 a 25 m resolution (European Copernicus mission, retrieved August 1, 2021, [https://land.copernicus.eu/imagery-](https://land.copernicus.eu/imagery-in-situ/eu-dem/eu-dem-v1.1)
178 [in-situ/eu-dem/eu-dem-v1.1](https://land.copernicus.eu/imagery-in-situ/eu-dem/eu-dem-v1.1)). Land use/ land cover percentages of all the delineated sub-catchments were
179 calculated from Corine Land Cover 2018 survey with a 25 ha spatial resolution (retrieved August 1, 2021,
180 <https://land.copernicus.eu/pan-european/corine-land-cover/clc2018?tab=mapview>). For data analysis, we
181 classified sub-catchments according to their dominant land cover (>50% of the total area) into forest (FOR),
182 cropland (CRP), grassland (GRA), and wetland (WET), and further differentiated sub-catchments with the
183 influence of settlement areas (S) and wastewater inflows (W). (Table 1). As drainage ditches (DD) in the Loisach
184 catchment were added as an extra land use category, this classification resulted in 9 land use classes (for details,
185 see Table 1).

186 2.3 Hydrological and water physico-chemical characteristics

187 In the Loisach and Schwingbach catchments, discharge was calculated (Gore, 2007) from stream depth
188 and velocity measurements using an electromagnetic sensor (OTT-MF-Pro, Hydromet, Germany). For streams in
189 the Neckar sub-catchments, velocity was measured using the electromagnetic sensor (OTT-MF-Pro, Hydromet,
190 Germany), and depth and discharge was obtained directly from gauging stations maintained by the water
191 authority of the state of Baden-Württemberg (<https://udo.lubw.baden-wuerttemberg.de/public/index.xhtml>). The
192 slope of a ~5 m reach at each sampling point was measured using a laser rangefinder with a slope function
193 (Nikon Model: 8381, Japan). The slopes and velocities were used to model the site-specific gas transfer
194 velocities (k in m d^{-1}) for the quantification of daily GHG fluxes per unit stream surface area ($\text{mass m}^{-2} \text{d}^{-1}$) (see
195 details in the flux calculation section).

196 Discharge measurements at each sampling location and every sampling event were complemented by *in*
197 *situ* measurements of water temperature ($^{\circ}\text{C}$), electrical conductivity ($\mu\text{S cm}^{-1}$), dissolved oxygen (DO) (mg L^{-1}),
198 and pH using the Pro DSS multiprobe (YSI Inc., USA). Water samples for nutrient and organic carbon analyses
199 were also collected and filtered on-site through polyethersulfone (PES) filters (0.45 μm pore size, pre-leached
200 with 60 ml of miliq water). The samples were stored in 30 ml acid-washed HDPE sample bottles in triplicates
201 and transported within 24 h to the laboratories at Karlsruhe Institute of Technology, Campus Alpin, Justus
202 Liebig University Giessen, or the University of Tübingen. On arrival, all samples were immediately frozen for
203 later analysis.

204 After unfreezing the samples overnight in a 4°C refrigerator, the samples were directly analyzed for
205 dissolved organic carbon (DOC), total dissolved nitrogen (TDN), nitrate ($\text{NO}_3\text{-N}$), and ammonium ($\text{NH}_4\text{-N}$)
206 concentrations. Dissolved organic nitrogen (DON) concentrations were estimated as the difference between the
207 TDN and dissolved inorganic nitrogen DIN ($\text{NO}_3\text{-N} + \text{NH}_4\text{-N}$) concentrations. DIN concentrations were
208 determined using colorimetric methods, and the absorbance of the samples was measured using a microplate
209 spectrophotometer (Model: Epoch, BioTek Inc., USA). $\text{NO}_3\text{-N}$ concentrations were analyzed based on reactions
210 with the Griess reagent (Patton & Kryskalla, 2011), and $\text{NH}_4\text{-N}$ concentrations were analyzed using the
211 indophenol method (Bolleter et al., 1961). The DOC concentrations were measured as non-purgeable organic

212 carbon (NPOC) using a TOC/ TN analyzer (Analytica-Jena; multi N/C 3100, Germany) after pre-treating the
 213 sample with 25% HCl acid to remove the dissolved inorganic carbon (DIC). The TDN concentrations were
 214 analyzed simultaneously with the same instrument (Analytica-Jena; multi N/C 3100, Germany).

215 2.4 Gas sampling, analysis, and calculations of annual areal fluxes

216 GHG stream, ditch, and wastewater samples were collected in triplicates simultaneously with the water
 217 physico-chemical samples using the headspace equilibration technique (Raymond et al., 1997). In brief, 80 ml of
 218 background water was equilibrated with 20 ml of atmospheric air in a syringe at *in situ* water temperatures. The
 219 headspace gas sample was transferred into 10ml glass vials for GHG concentration analysis in the laboratory of
 220 the Karlsruhe Institute of Technology, Campus Alpin (see full sampling details in Mwanake et al., 2022).
 221 Atmospheric air samples were taken twice (morning and afternoon) on each sampling day to correct for
 222 background atmospheric GHG concentrations. GHG concentrations from the headspace were analyzed using an
 223 SRI gas chromatograph (GC) (8610C, Germany) with an electron capture detector (ECD) for N₂O and a flame
 224 ionization detector (FID) with an upstream methanizer for simultaneous measurements of CH₄ and CO₂
 225 concentrations. The standards used for the GC calibration were 450, 800, 1000, 1500, 2000, and 3000 ppm for
 226 CO₂, 1, 2, 3, 4, 5, and 6 ppm for CH₄ and 0.4, 0.8, 1, 1.5, 2, and 3 ppm for N₂O. Dissolved GHG concentrations
 227 in the stream water were calculated from post-equilibration gas concentrations in the headspace after correcting
 228 for atmospheric (ambient) GHG concentrations (e.g., Aho et al., 2019; Mwanake et al., 2022).

229 Daily diffusive fluxes (F) (moles m⁻² d⁻¹) of the GHGs were estimated using Fick's Law of gas
 230 diffusion, where the F is the product of the gas exchange velocity (k) (m d⁻¹) and the difference between the
 231 stream water (C_{aq}) (moles m⁻³) and the ambient atmospheric gas concentration in water assuming equilibrium
 232 with the atmosphere (C_{sat}) (moles m⁻³) (Equation 1). GHG concentrations and fluxes were expressed in mass
 233 units by multiplying by the respective molar masses.

$$234 \quad F = k (C_{aq} - C_{sat}) \quad (1)$$

235 The temperature-specific gas transfer velocities (k) for each of the gases were calculated from
 236 normalized gas transfer velocities (k_{600}) (m d⁻¹) (corresponding to the k of CO₂ at 20° C with a Schmidt number
 237 of 600) and temperature-dependent Schmidt numbers (Sc) (unit-less) of the respective gases (Equation 2).

$$238 \quad k = k_{600} \times (600/Sc)^{0.5} \quad (2)$$

239 The k_{600} was modeled using Equation 3 (drawn from Equation 4 in Table 2 of Raymond et al. (2012)), which was
 240 calibrated from headwater streams of similar characteristics as our study sites, where V is stream velocity (m s⁻¹),
 241 and S is the slope (m m⁻¹).

$$242 \quad k_{600} = VS^{0.76} \times 951.5 \quad (3)$$

243 Before choosing the equation above for modeling the k_{600} values, we compared the k_{600} values
 244 calculated from all seven empirical models by Raymond et al. (2012). The predicted k_{600} values from models 3,
 245 4, 5, and 6 in Table 2 of Raymond et al. (2012), which all use velocity and slope as input parameters, were
 246 mainly similar for the three discharge periods and across all stream orders 1–6 (ANOVA; $p > 0.05$). In contrast,
 247 the calculated k_{600} values from equations 1, 2, and 7, which use a stream depth parameter, were higher (ANOVA;

248 $p < 0.05$), particularly from the higher stream orders (5–6). This finding is inconsistent with the energy dissipation
249 model of turbulent streams where k_{600} is predicted to decrease with stream order. We, therefore, interpreted this
250 to indicate a breakdown of these models for higher stream orders. This also agrees with Raymond et al. (2012)
251 recommendations, and we, therefore, choose not to use models 1, 2, and 7 for this study. Out of the remaining
252 equations, 3, 4, 5, and 6, we used equation 4, which calculated k_{600} based on the slope and velocity parameters
253 and was also in line with several previous studies spanning a wide range of stream orders similar to our study.
254 (See, Aho et al., 2019; Borges et al., 2019; Mwanake et al., 2019; Hall & Ulseth, 2020; Aho et al., 2021;
255 Mwanake et al., 2022). The uncertainties in the modeled gas transfer velocities were reduced in this study by
256 parametrizing the velocities and slopes based on actual field measurements of both variables. Equation 3 also
257 estimated the gas transfer velocities in the drainage ditches with a measurable flow velocity and slope.

258 Water-to-atmosphere fluxes for all three GHGs across all land use classes in each sub-catchment were
259 calculated from the mean daily CO_2 , CH_4 , and N_2O fluxes during different discharge conditions. Total GHG
260 fluxes were expressed as CO_2 equivalents emissions ($\text{mg CO}_2\text{-eq m}^{-2} \text{d}^{-1}$) computed from global warming
261 potentials (GWP_{100}) using 28 for CH_4 and 298 for N_2O (IPCC, 2014). We followed the procedure developed in
262 Mwanake et al. (2022) to scale tri-weekly measurements to annual flux estimates. Briefly, we classified each
263 sampling date of every location into low, medium, or high discharge conditions according to whether normalized
264 discharge fell in the 0–33% percentile (low), 34–66% (medium), or 67–100% (high) days. Normalized discharge
265 for each site was determined by dividing each absolute discharge measurement for every site visit during the
266 year by the maximum measured discharge. The number of days in each discharge period was estimated as the
267 ratio of observations in each discharge period to the total number of flux observations in individual land use
268 classes in each catchment. CO_2 equivalents fluxes were then calculated for the three different discharge periods
269 in each land use class by multiplying the daily mean CO_2 equivalents flux measured during each period and the
270 number of days within each period. Annual fluxes were finally estimated by summing up the emissions of the
271 low, medium, and high discharge periods for the individual land use classes in each catchment.

272 2.5 Statistical analysis

273 Linear mixed-effects models were used to investigate the effect of seasonality and land use on water
 274 physico-chemical variables, GHG concentrations, and fluxes (“lme4” package in R version 4.1.1). Fixed effects
 275 in the models consisted of land use classes in each catchment (Table 1) and seasons: summer June 1–August 31,
 276 autumn September 1–November 30, winter December 1–February 28, and spring March 1–May 31. Random
 277 effects accounting for repeated measures were also included in the models. Model performance was assessed
 278 based on the distribution of residuals (i.e., residuals should be normally distributed with a mean close to zero)
 279 and conditional r^2 values calculated from significant models (p-value <0.05) (“MuMIn” package in R). A Tukey
 280 post-hoc test (p-value <0.05) of least-square means was used on the mixed models to identify individual
 281 differences within each categorical fixed effect. GHG concentration and flux data and other water physico-
 282 chemical variables were transformed using the natural logarithm to meet the assumption of normality. Because
 283 we quantified occasional negative fluxes in some of our sites, constant flux values of $50 \text{ mg m}^{-2} \text{ d}^{-1}$ for $\text{CO}_2\text{-C}$,
 284 $0.5 \text{ mg m}^{-2} \text{ d}^{-1}$ for $\text{CH}_4\text{-C}$, and $10 \text{ } \mu\text{g m}^{-2} \text{ d}^{-1}$ for $\text{N}_2\text{O-N}$ were added to the fluxes to enable the natural logarithm
 285 transformations.

286 Path analysis from structural equation models (SEMs, “lavaan” package in R version 4.1.1) was used to
 287 determine how environmental factors linked to seasonality and land use directly or indirectly influenced
 288 *instream* GHG production and consumption processes as well as external GHG sources, i.e., dissolved GHG
 289 inputs to the streams originating from either wastewater inflows or terrestrial landscapes which were not
 290 produced *in situ*. In brief, these SEMs were constructed based on causal relationships between environmental
 291 variables (interpreted as ultimate drivers of GHG concentrations) and substrate variables, which are affected by
 292 the environmental variables and also act as immediate drivers that affect GHG concentrations. Substrate
 293 variables in the models, which are known to influence *in situ* biogeochemical GHG production and consumption
 294 processes directly, included dissolved oxygen DO (% saturation), DOC (mg L^{-1}), $\text{NH}_4\text{-N}$ (mg L^{-1}), and $\text{NO}_3\text{-N}$
 295 (mg L^{-1}) concentrations (Battin et al., 2008; Stanley et al., 2016; Quick et al., 2019). The environmental variables
 296 in the models, which influence *in situ* GHG concentrations either directly by facilitating dissolved GHG inputs
 297 or indirectly by controlling the substrate variables, were water temperature ($^{\circ}\text{C}$) (a proxy for different seasons),
 298 stream velocity V (m s^{-1}), % upstream agricultural area for each sampling point (AGR: grassland + cropland
 299 area) and wastewater inflows (WW: Boolean numbers, i.e., 1 for the presence of wastewater inflow and 0 for
 300 absence).

301 The hypothesized relationships between the substrate and environmental drivers of instream GHG
 302 concentrations were assessed in the overall theoretical SEM, which comprises several multivariate regression
 303 equations shown in Equations 4-8. To get the best-fit SEM, the removal of parts of the theoretical SEM was done
 304 manually until the model with the highest parsimony fit index (PNFI) and a root mean squared error of
 305 approximation (RMSEA) of ≤ 0.05 was found (Schumacker and Lomax, 2016). Graphical representations of the
 306 significant relationship pathways from the best-fit model, including standardized slope parameter estimates, were
 307 done using the “semPlot” package in R software.

$$308 \quad \text{Log}_e \text{ GHG concentration} = \text{DO} + \text{DOC} + \text{stream velocity} + \text{water temperature} + \text{Log}_e \text{NO}_3 +$$

$$309 \quad \text{Log}_e \text{NH}_4 + \text{wastewater inflow} + \text{agricultural area}$$

310 (4)

311 $\text{Log}_e \text{NO}_3 = \text{DO} + \text{Log}_e \text{NH}_4 + \text{DOC} + \text{wastewater inflow} + \text{agricultural area} +$
312 stream velocity (5)

313 $\text{Log}_e \text{NH}_4 = \text{DO} + \text{DOC} + \text{wastewater inflow} + \text{agricultural area} +$
314 stream velocity (6)

315 $\text{DOC} = \text{wastewater inflow} + \text{agricultural area} + \text{stream velocity}$ (7)

316 $\text{DO} = \text{DOC} + \text{wastewater inflow} + \text{agricultural area} + \text{stream velocity}$ (8)

Table 1: Summary descriptions of sampling sites located in the Schwingbach, Loischach, and Neckar sub-catchments (Goldersbach, Ammer and Steinlach) (Fig. 1). The land use (%) was calculated for the site-specific upstream sub-catchments based on the Corine Land Cover 2018 survey of Europe (See main text for details).

Main Catchment	Site	Stream order	Coordinates (decimal degrees)		Sub-catchment area (Ha)	Elevation at sampling point	Sub-catchment Landuse / landcover (%)			Wastewater inflow	Main sub-catchment landuse class	Main land use Abbreviations	
			Latitude	Longitude			Forest	Wetland	Grassland				Cropland
Loischach	Stream	1	47.5694	11.1554	4	651	40	60	0	0	0	Wetland	WET
Loischach	Stream	2	47.5689	11.1556	10	645	22	78	0	0	0	Wetland	WET
Loischach	Stream	1	47.5440	11.1193	11	660	0	0	100	0	0	Grassland	GRA
Loischach	Stream	1	47.5399	11.1105	13	663	19	0	81	0	0	Grassland	GRA
Loischach	Stream	1	47.4670	11.0537	40	750	86	0	14	0	0	Forest	FOR
Loischach	Stream	2	47.4691	11.0394	75	756	99	0	0	1	0	Forest	FOR
Loischach	Stream	2	47.5858	11.1429	102	719	100	0	0	0	0	Forest	FOR
Loischach	Drainage ditch		47.5963	11.1730	11	630	27	0	73	0	0	Drainage ditch	DD
Loischach	Drainage ditch		47.5953	11.1657	11	645	43	57	0	0	0	Drainage ditch	DD
Loischach	Drainage ditch		47.5696	11.1550	17	630	47	0	53	0	0	Drainage ditch	DD
Schwingbach	Stream	1	50.5051	8.6127	41	297	96	0	0	4	0	Forest	FOR
Schwingbach	Stream	1	50.4695	8.6179	60	187	0	0	0	100	0	Cropland	CRP
Schwingbach	Stream	2	50.4811	8.5407	62	241	98	0	2	0	0	Forest	FOR
Schwingbach	Stream	1	50.4756	8.5472	67	334	86	0	0	14	0	Forest	FOR
Schwingbach	Stream	2	50.4922	8.5971	220	260	47	0	0	53	0	Cropland	CRP
Schwingbach	Stream	2	50.5032	8.5553	220	272	65	0	0	35	0	Forest	FOR
Schwingbach	Stream	2	50.4887	8.5555	268	204	83	0	0	17	0	Forest	FOR
Schwingbach	Stream	1	50.4669	8.5792	355	207	14	0	0	84	2	Cropland	CRP
Schwingbach	Stream	3	50.5050	8.6148	2337	183	37	0	6	48	9	Cropland+settlement	CRP_S
Schwingbach	Stream	3	50.5166	8.5992	5345	189	44	0	4	45	7	Cropland+settlement	CRP_S
Goldersbach (Neckar)	Stream	5	48.5588	9.0591	11623	367	97	0	0	3	0	Forest	FOR
Ammer (Neckar)	Stream	5	48.5649	8.8986	26157	379	11	0	1	84	4	Cropland+settlement	CRP_S
Ammer (Neckar)	Stream	6	48.5640	8.8997	26361	377	11	0	1	83	5	Cropland+settlement+wastewater	CRP_S_W
Ammer (Neckar)	Stream	6	48.5271	8.9615	30441	348	14	0	2	77	8	Cropland+settlement	CRP_S
Steinlach/Neckar	Stream	6	48.4796	9.0634	51332	348	74	0	10	11	4	Forest+settlement	FOR_S
Steinlach/Neckar	Stream	6	48.4812	9.0639	51332	344	74	0	10	11	4	Forest+settlement+wastewater	FOR_S_W
Ammer/Neckar	Wastewater effluent		48.5644	8.8993								Wastewater	WWA
Steinlach/Neckar	Wastewater effluent		48.4805	9.0636								Wastewater	WWS

318 3 Results

319 3.1 Hydrological variables

320 Across all sampling points and seasons, tri-weekly sampled stream velocity measurements (annual
321 mean \pm SE) were two-folds higher for streams ($0.19 \pm 0.009 \text{ m s}^{-1}$, range: 0.01- 1.17) than ditches ($0.05 \pm 0.06 \text{ m}$
322 s^{-1} , range: 0.01–0.23) (Fig A1). Seasonality had an overall significant effect (p-value <0.05) on stream velocities
323 across all sampling points, with higher stream velocities observed in spring ($0.24 \pm 0.02 \text{ m s}^{-1}$) than in autumn
324 ($0.12 \pm 0.01 \text{ m s}^{-1}$) (Table 2; Table B2). Discharge in streams ($3.9\text{--}18,500 \text{ L s}^{-1}$) and in ditches ($0.1\text{--}37 \text{ L s}^{-1}$) was
325 highly variable, reflecting differing stream sizes and seasonal variability (Fig. A1). The Neckar sub-catchments,
326 dominated by streams (orders 5 - 6), had an order of magnitude higher mean annual discharge ($874.7 \pm 178 \text{ L s}^{-1}$)
327 than the streams in the other catchments (Loisach: $50.5 \pm 6 \text{ L s}^{-1}$ and Schwingbach: $26.7 \pm 4 \text{ L s}^{-1}$). The
328 average discharge at the stream and ditch sampling points in all our study catchments were 3 to 5-fold higher in
329 spring and summer (384.1 ± 96 and $526.4 \pm 171 \text{ L s}^{-1}$, respectively) than in autumn and winter (86.25 ± 13.07
330 and 157.3 ± 31.58 , respectively; p-value <0.01 ; Table 2; Table B2).

331 Table 2: Results of multiple linear mixed-effects models predicting the effect of seasonality (summer, autumn,
 332 winter, and spring) and sub-catchment land use (Table 1) on stream velocity, discharge, water physico-chemical
 333 variables, GHG concentration, gas-transfer velocity, and GHG flux. The model performance was assessed based
 334 on conditional r^2 and the distribution of residuals, including the variances explained by fixed effects and repeated
 335 measures' random effects.

Dependent variables	Conditional r^2	Type 2 ANOVA table	
		Season (df=3)	Land use (df=11)
		F-statistic/significance	F-statistic/significance
Water physico-chemical and hydrological variables			
Temperature ($^{\circ}$ C)	0.87	66.3***	9.1***
pH	0.80	3.1*	97.8***
DO (mg L^{-1})	0.83	20.1***	143.7***
Electrical Conductivity ($\mu\text{s cm}^{-1}$)	0.83	4.9**	86.1***
$\text{NO}_3\text{-N}$ (mg L^{-1}) ^a	0.80	4.9**	141***
$\text{NH}_4\text{-N}$ (mg L^{-1}) ^a	0.60	ns	32.3***
TDN (mg L^{-1}) ^a	0.79	5.6**	93.8***
DON (mg L^{-1}) ^a	0.55	ns	13.9***
DOC (mg L^{-1}) ^a	0.59	ns	47.3***
DOC:DIN	0.84	3.2*	133.2***
DOC:DON	0.63	ns	15.1***
Velocity ^a	0.59	3.7*	34.5***
Discharge ^a	0.86	4.6**	96.9***
k₆₀₀, Gas concentration and flux			
$\text{CO}_2\text{-C}$ concentration ($\mu\text{g L}^{-1}$) ^a	0.86	25.6***	219.3***
$\text{CH}_4\text{-C}$ concentration ($\mu\text{g L}^{-1}$) ^a	0.89	ns	273.1***
$\text{N}_2\text{O-N}$ concentration (ng L^{-1}) ^a	0.75	3.3*	69***
k_{600} (m d^{-1}) ^a	0.57	ns	31.2***
$\text{CO}_2\text{-C}$ flux ($\text{mg m}^{-2} \text{d}^{-1}$) ^a	0.57	ns	50.2***
$\text{CH}_4\text{-C}$ flux ($\text{mg m}^{-2} \text{d}^{-1}$) ^a	0.79	ns	113***
$\text{N}_2\text{O-N}$ flux ($\mu\text{g m}^{-2} \text{d}^{-1}$) ^a	0.70	3.9*	75.6***
Total fluxes $\text{CO}_2\text{-eq}$ ($\text{g m}^{-2} \text{d}^{-1}$) ^a	0.67	ns	67***
Level of significance (p-value)	^a Natural logarithm transformation		
* <0.05			
** <0.01			
*** <0.001	Conditional r^2 = Variance explained by fixed and random effects of sampling date		
ns >0.05	df= degrees of freedom		

336

337

338 3.2 Water physico-chemical variables

339 3.2.1 Seasonal variation

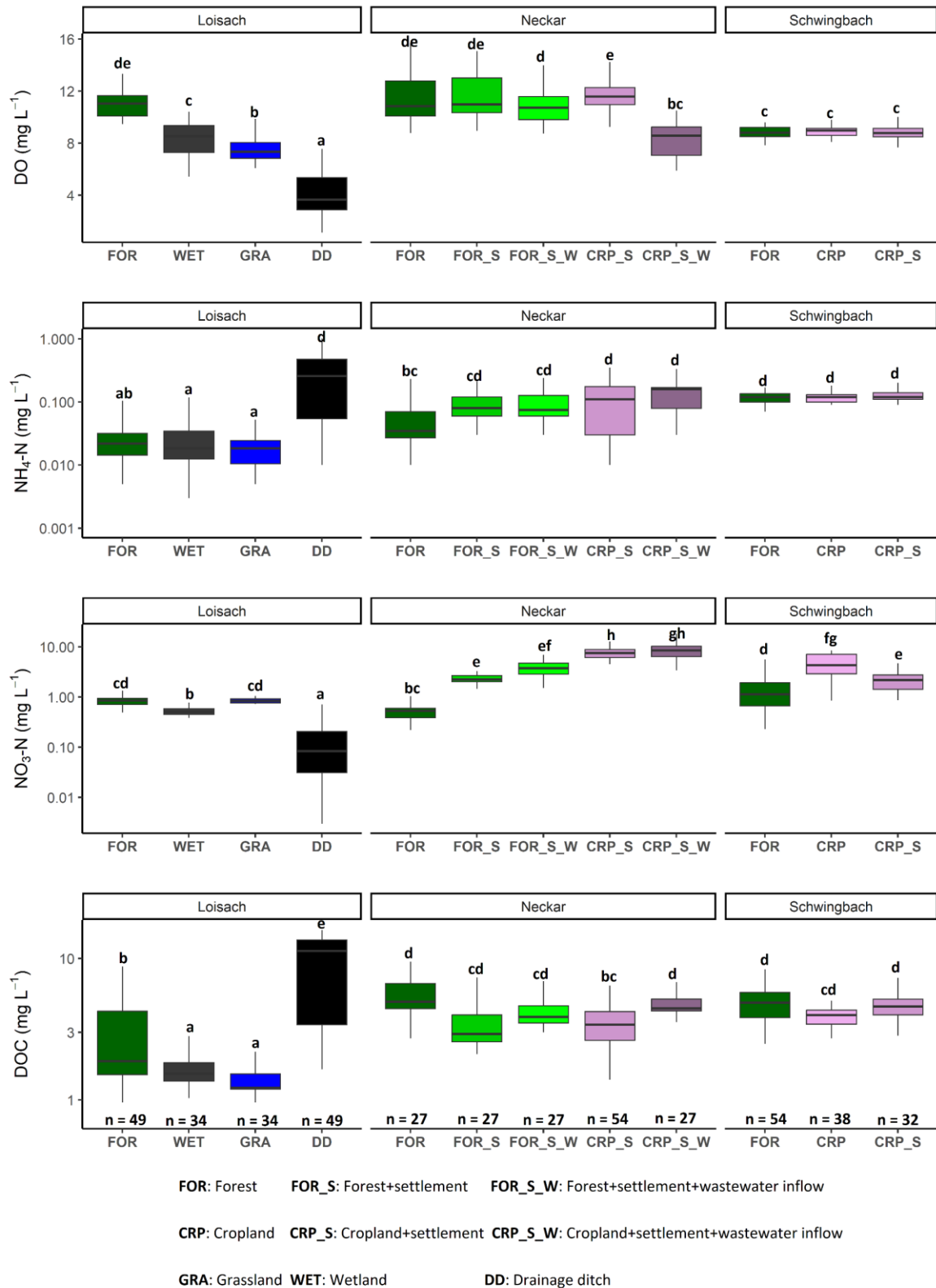
340 Water temperature, DO, and pH ranged from 0.9–24 $^{\circ}$ C, 1.1–15.7 $\text{mg O}_2 \text{L}^{-1}$ and 6.7–9.0, respectively.
 341 Streams in the mountainous Loisach catchment had a mean annual (\pm SE) water temperature of 9.0 ± 0.2 $^{\circ}$ C,
 342 which was ~ 1 $^{\circ}$ C colder than streams of the Schwingbach catchment (10.0 ± 0.4 $^{\circ}$ C) and 3 degrees colder than
 343 streams in the Neckar sub-catchments (12.0 ± 0.3 $^{\circ}$ C). The annual ranges of $\text{NH}_4\text{-N}$, $\text{NO}_3\text{-N}$, DON, TDN, and
 344 DOC concentrations across all catchments were 0.05–1.0 mg L^{-1} , 0.5–14.8 mg L^{-1} , 0.05–10.9 mg L^{-1} , 0.6–17.0

345 mg L⁻¹, and 0.9–16.0 mg C L⁻¹, respectively. DO, NO₃ and TDN concentrations showed significant seasonal
346 variability (Table 2, Table B2). DO was higher in winter and spring than in summer and autumn (p-
347 value<0.001). NO₃-N and TDN concentrations were highest in winter and lowest in autumn and summer (p-
348 value<0.01), while NH₄-N, DOC, and DON showed no significant seasonal variation (p-value>0.05; Table 2;
349 Table B2). We additionally calculated DOC: DIN and DOC: DON molar ratios, which had interquartile ranges
350 from 0.9–4.9 and 4.1–29.0, respectively. DOC: DIN ratios showed significant seasonal variability, with higher
351 values in summer and spring than in winter (p-value<0.05), while no seasonal variability was found for DOC:
352 DON ratios (p-value>0.05; Table 2: Table B2).

353 3.2.2 Land use variation

354 Catchment land use was more significant than seasonality in explaining the variability of most water
355 physico-chemical variables (p-value<0.001; Table 2). In the Loisach catchment, ditches had up to 2.6 times
356 lower DO and 8 times lower NO₃-N concentrations than the streams across all land use types (Fig. 2; Table B3).
357 In contrast, NH₄-N and DOC concentrations, as well as the DOC: DIN ratio, were 6-10 times higher in the
358 ditches than in the streams (Fig. 2; Table B3). In the Neckar sub-catchments, forested streams had 1-2 times
359 higher DO and DOC concentrations than cropland, settlement, and wastewater-influenced streams. The opposite
360 was true for NO₃-N and DON concentrations, which were an order of magnitude higher in the cropland,
361 settlement, and wastewater-influenced streams than in the forested streams (Fig. 2; Table B3). As a result, DOC:
362 DIN and DOC: DON ratios in the Neckar sub-catchments were, therefore, higher in forested streams than in
363 cropland, settlement, and wastewater-influenced streams (Table B3).

364 In addition, cropland streams directly receiving wastewater inflows also had significantly lower DO and
365 higher DOC than cropland streams without wastewater inflows (Fig. 2; Table B3). While NO₃-N and DON
366 concentrations were not significantly different in cropland streams with or without wastewater inflows, the
367 concentrations of both variables were slightly higher in cropland streams with wastewater inflows (Table B3). In
368 streams of the Schwingbach catchment, surrounding croplands and settlement areas also influenced NO₃-N
369 concentrations, which were up to 3-fold higher than in the forested streams. Across all the three catchments, DO
370 concentrations, DOC: DIN and DOC: DON ratios were higher in the forested streams and decreased in streams
371 of sub-catchments with predominant agricultural land uses or settlement areas, while the opposite was found for
372 NO₃-N and DON concentrations (Table B3). Additionally, forested streams in the Loisach catchment had an
373 order of magnitude higher DOC: DON ratios than forested streams in the Neckar and Schwingbach catchments
374 (Table B3).



375

376 Fig. 2: Boxplots of DO, NH₄-N, NO₃-N, and DOC concentrations in stream and ditch waters in the three
 377 catchments grouped by dominating land uses (see Table 1 methods). Letters on top of the boxplots represent
 378 significant differences ($p < 0.05$) among land use classes across the three catchments based on Tukey post-hoc
 379 analyses from the linear mixed-effects model results (Table 2).

380 3.3 GHG concentrations and fluxes

381 3.3.1 Seasonal variation

382 In all headwater streams, CH₄ and N₂O concentrations varied greatly, spanning three orders of
 383 magnitude, i.e., from 0.03– 58 µg-C L⁻¹ (*p*CH₄ 1.3–2,145 µatm) for CH₄ and from 20–18,717 ng-N L⁻¹ (*p*N₂O
 384 21– 15,813 natm) for N₂O. In contrast, CO₂ concentrations varied less, spanning only one order of magnitude
 385 from 219–4,868 µg-C L⁻¹ (*p*CO₂ 369–7,979 µatm). GHG concentrations in ditches also varied widely, with CH₄,
 386 N₂O and CO₂ concentrations spanning 1-2 orders of magnitude ranging from 27–831 µg-C L⁻¹ (*p*CH₄ 1,469–
 387 34,482 µatm), 56–1,540 ng-N L⁻¹ (*p*N₂O 35–1,512 natm), and 1,722– 9,746 µg-C L⁻¹ (*p*CO₂ 2,888–13,400
 388 µatm), respectively (Fig. A2, A3).

389 Streams and drainage ditches across all seasons were predominantly sources of atmospheric CH₄, N₂O,
 390 and CO₂, as indicated by concentrations mostly above the atmospheric background and the positive flux values
 391 displayed in Figure 3. CO₂ fluxes from streams ranged from -0.05–179 g C m⁻² d⁻¹ (mean 19 g C m⁻² d⁻¹), CH₄
 392 fluxes ranged from -0.40–325 mg C m⁻² d⁻¹ (mean 30 mg C m⁻² d⁻¹), and N₂O fluxes ranged from -9.2–199.5 mg
 393 N m⁻² d⁻¹ (mean 12 mg N m⁻² d⁻¹). CO₂ and CH₄ fluxes from the ditches varied between 2–63 g C m⁻² d⁻¹ (mean
 394 13.7 g C m⁻² d⁻¹) and from 117–7,933 mg C m⁻² d⁻¹ (mean 1,532 mg C m⁻² d⁻¹), respectively, while N₂O fluxes
 395 ranged from -0.8–7.1 mg N m⁻² d⁻¹ (mean 1.2 mg N m⁻² d⁻¹).

396 Seasonal variations in GHG concentrations and fluxes were GHG-dependent and varied across the land
 397 uses within each catchment (Fig. 3; Fig. A2). In the Loisach catchment, there was a decline in *instream* CO₂
 398 concentrations in the summer, followed by a subsequent increase in autumn, particularly at non-forested
 399 sampling points (Fig. A2). Similar *instream* CO₂ concentration trends, with lower values in the summer season
 400 and increasing values in autumn, were also found for non-forested streams of the Neckar sub-catchments (Fig.
 401 A2). However, non-forested streams of the Schwingbach catchments showed slightly different trends, with a
 402 decline in CO₂ concentrations in spring and an increase in CO₂ concentrations in the late summer. (Fig. A2).
 403 Considering all data over all catchments, seasonality had an overall significant effect on CO₂ (*p*-value < 0.001),
 404 with summer concentrations being 1.6 times lower than in autumn, while CO₂ fluxes showed no significant
 405 seasonal variability (*p*-value > 0.05; Table 2; Table B2).

406 In contrast to CO₂, N₂O concentrations in the Loisach and Schwingbach catchments decreased from
 407 summer to autumn but increased again towards the beginning of winter (Fig. A2). In autumn, N₂O
 408 concentrations at first and second-order forested streams in the Loisach and Schwingbach catchments were often
 409 below atmospheric concentrations (Fig. A2), characterizing these sites as N₂O sinks (Fig. 3). A similar autumn
 410 decline in N₂O concentrations was not observed in the streams of the Neckar sub-catchments, but rather, N₂O
 411 concentrations increased from autumn to winter (Fig. A2). Across all catchments and sampling points, N₂O
 412 concentrations were 2.4 times higher in winter than in the other seasons (*p*-value < 0.05; Table B2). N₂O fluxes
 413 were up to 1.6 times higher in summer and winter than in autumn and spring (*p*-value < 0.05; Fig. 3; Table B2),
 414 which represented periods of either high N₂O concentrations and moderate gas transfer velocities (winter) or
 415 moderate N₂O concentrations and high gas transfer velocities (summer) (Table B2).

416 CH₄ concentrations showed a seasonal pattern only in the Schwingbach catchment (Fig. A2), which
 417 showed a decline from summer through autumn and winter. This trend was not observed for the other
 418 catchments (Fig. A2) and resulted in a non-significant seasonal effect on both concentrations and fluxes when all
 419 data from all catchments were considered together (p-value>0.05; Table 2; Table B2). Overall, GHG fluxes from
 420 streams within human-influenced land use classes (grasslands, croplands, and settlement areas) were more
 421 temporally variable (annual coefficient of variation > 55 %) than those in sub-catchments dominated by forests or
 422 wetlands (Fig. 3).

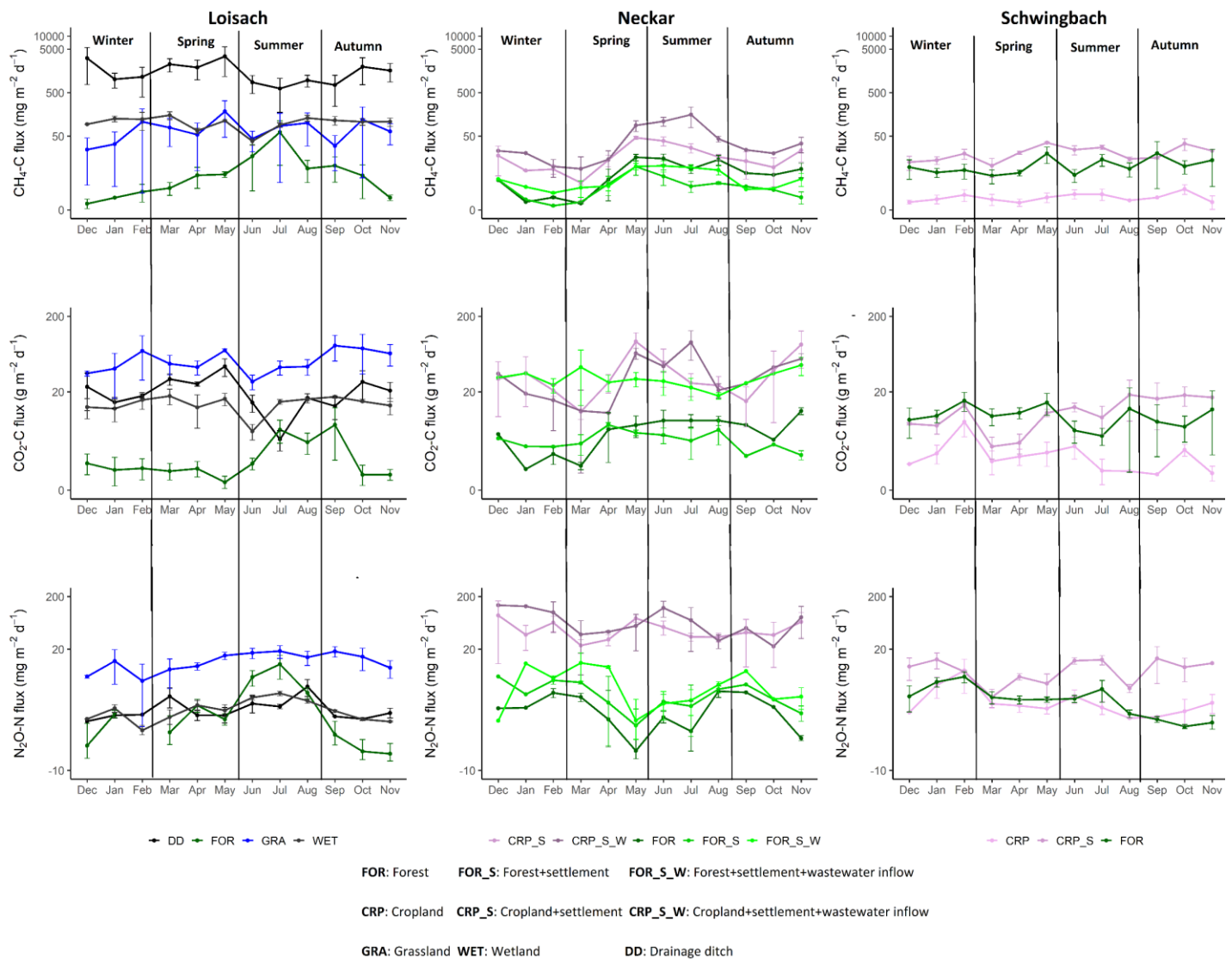


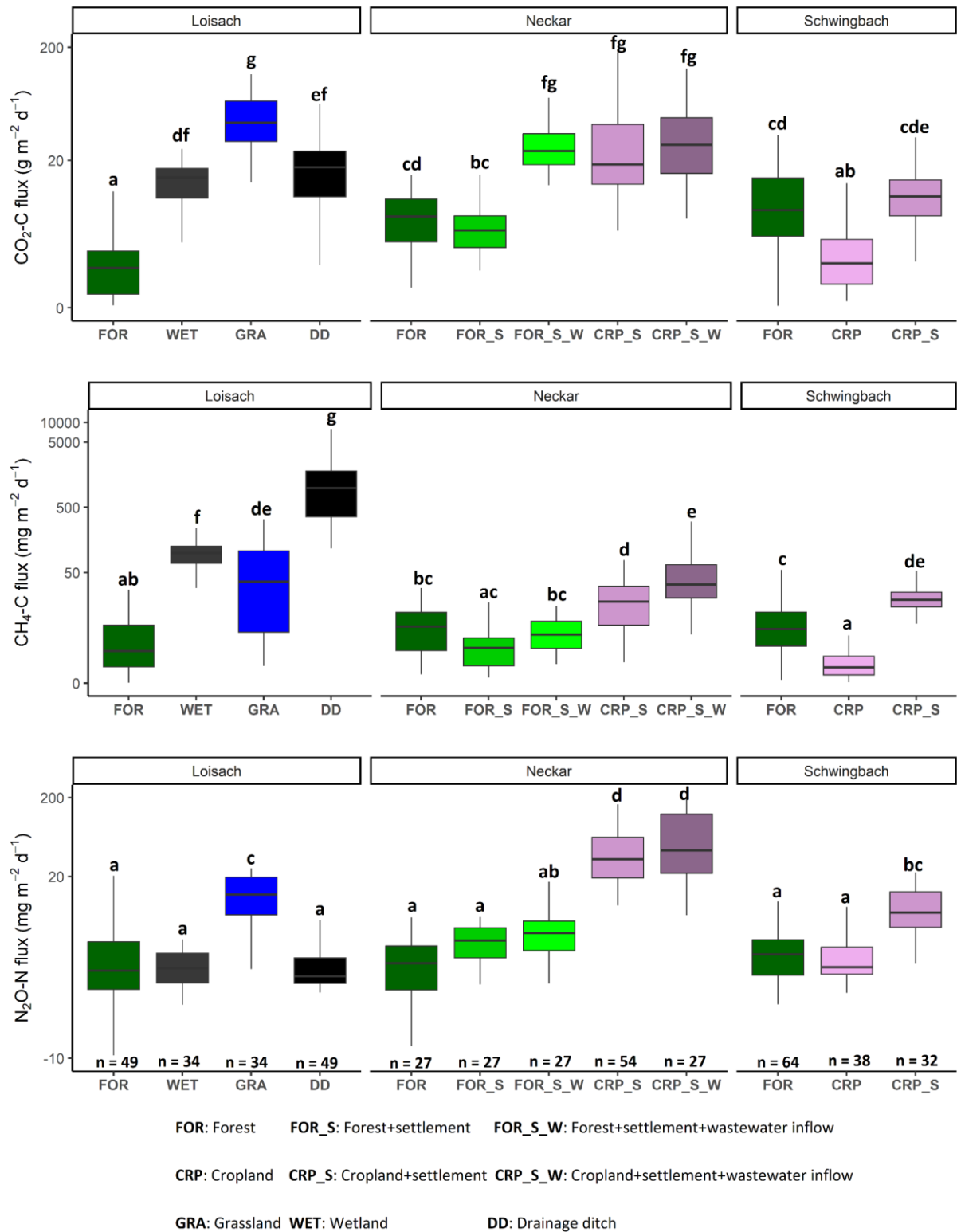
Fig. 3: Monthly mean \pm SE of CO₂, CH₄, and N₂O fluxes across all 26 sampled streams and ditches in the Loisach, Neckar, and Schwingbach catchments (see Table 1 methods). The colors of the lines and labels on the graph indicate the nine dominant land use classes.

423 3.3.2 Land use variation

424 Like water physico-chemical variables, the variability in GHG concentrations and fluxes was more
425 strongly linked to catchment land use than seasonality (p -value <0.001 ; Table 2). In the Loisach catchment, CO₂
426 concentrations and fluxes were an order of magnitude higher for the ditch and stream sites dominated by
427 grassland land uses than forested-dominated sites (Fig. 3; Fig. 4; Table B3). N₂O concentrations and fluxes in
428 streams were also an order of magnitude higher in the grassland streams compared to the wetland and forested
429 ones, with the latter functioning as occasional sinks for atmospheric N₂O (Fig. 3; Fig. 4; Table B3). Wetland
430 streams had higher CH₄ fluxes than the other streams (Fig. 3; Fig. 4; Table B3). Overall, ditches showed up to 14
431 times more elevated CO₂ and up to 850 folds higher CH₄ concentrations than the streams of the Loisach
432 catchment (Fig. A3; Table B3). In contrast, N₂O concentrations in the ditches were highly variable, with higher
433 and lower than atmospheric concentrations over the sampling year (Fig. A2,A3). CH₄ fluxes were two orders of
434 magnitude higher in ditches than in streams (Fig. 3; Fig. 4; Table B3). Interestingly, the ditches were even more
435 often N₂O sinks than forests, which resulted in the overall lowest N₂O fluxes, e.g., 10 times lower than the ones
436 of grassland-dominated streams (Fig. 3; Table B3)

437 In the Neckar sub-catchments, CO₂, CH₄, and N₂O concentrations and fluxes were 1-10 times higher in
438 the streams located in cropland and settlement areas as compared to streams in forested areas (Fig. 3; Fig. 4; Fig.
439 A3; Table B3). Generally, GHG concentrations and fluxes of streams in cropland and settlement areas further
440 increased if wastewater inflows affected sampling points (Fig. 3; Fig. 4; Fig. A3; Table B3). For the latter, it is
441 noteworthy that pronounced differences in wastewater characteristics existed in our study, even though the
442 treatment procedures and the number of served households (80000) were comparable for the two wastewater
443 treatment plants. Overall, the wastewater outflow in the Ammer catchment had higher TDN, DOC, CH₄, and
444 N₂O concentrations than the Steinlach catchment's (Table B1). In contrast to the other two catchments, forested
445 streams in the Schwingbach catchment had CO₂ and CH₄ concentrations and fluxes comparable to cropland and
446 settlement-influenced streams within the catchment (Fig. 3; Fig. 4; Fig. A3; Table B3). However, N₂O
447 concentrations and fluxes were higher in streams with cropland and settlement influences than in forested
448 streams (Fig. 3; Fig. 4; Fig. A3; Table B3).

449 In addition to land use effects, we also examined spatial variability in the GHG concentrations and
450 fluxes linked to stream order differences. We found tendencies of higher CO₂, CH₄, and N₂O concentrations and
451 fluxes with increasing stream orders in the Schwingbach and Neckar catchments dominated by croplands and
452 settlement areas. In contrast to the Neckar and Schwingbach catchments, GHG concentrations and fluxes in the
453 more natural Loisach catchment decreased with stream order (Fig. A4). Comparing across catchments, higher
454 stream orders (5&6) in the human-influenced Neckar catchment had higher or comparable GHG concentrations
455 and fluxes than lower stream orders (1–3) in the Schwingbach and Loisach catchments (Fig. A4).



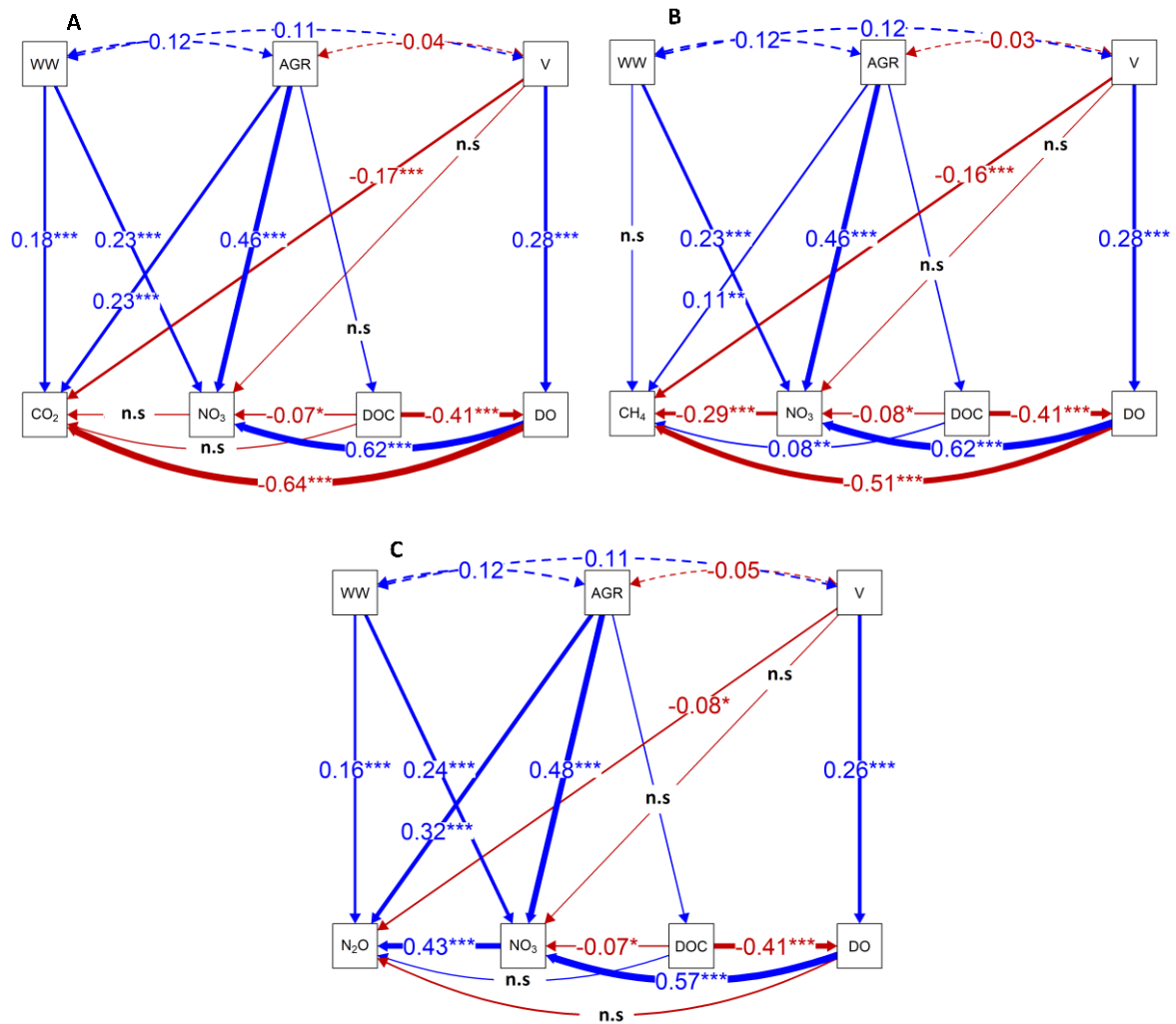
456

457 Fig. 4: Boxplots of CO₂, CH₄, and N₂O fluxes in stream and ditch waters in the three catchments grouped by land
 458 uses (see Table 1 methods). Letters on top of the boxplots represent significant differences (p<0.05) amongst the
 459 land use classes across the three catchments based on Tukey post-hoc analyses from the linear mixed-effects
 460 models' results (Table 2).

461 3.4 Direct and indirect drivers of greenhouse gas concentrations

462 We used path analyses from best-fit SEMs based on all our datasets to explain how environmental
463 factors such as upstream agricultural area, wastewater inflow, and stream velocity controlled the spatial-temporal
464 dynamics of GHG concentrations that drove the fluxes. The slopes parameter estimates from the SEMs revealed
465 significant (p -value <0.05) interactions between the environmental variables and DO (% saturation), DOC mg L⁻¹,
466 and NO₃-N mg L⁻¹, i.e., substrate variables that directly control *in situ* GHG concentrations (Fig. 5, Table B4). In
467 contrast to all other variables, water temperature and NH₄-N mg L⁻¹ did not contribute significantly (p -
468 value >0.05) to the variance explained by the best-fit SEMs and were removed from the final path analyses
469 (Table B4). That said, an increase in the upstream agricultural area resulted in a ~46% increase in *in situ* NO₃-N
470 concentrations. Wastewater inputs resulted in a ~23% increase in *in situ* NO₃ concentrations, while DOC
471 concentrations were not significantly affected. DO decreased with increasing DOC concentrations, while NO₃-N
472 concentrations followed an opposite pattern and increased with increasing DO concentrations (Fig 5).

473 CO₂ and CH₄ concentrations had a negative relationship with DO (Fig 5A-B), but N₂O concentrations
474 were not significantly related to DO (Fig 5C). Besides DO, CO₂ concentrations decreased by 17% with stream
475 velocity, increased by 18% with wastewater inflows, and increased by 23% with upstream agricultural area (Fig
476 5A). CH₄ concentrations also decreased by 16% with increasing stream velocity. However, the effect of the
477 increased share of agricultural areas (+11%) on CH₄ concentrations was lower than for CO₂. Additionally, CH₄
478 concentrations also decreased by 29% with increasing NO₃-N concentrations (Fig. 5B). In contrast to CO₂ and
479 CH₄, N₂O concentrations increased by 43% with increasing NO₃-N concentrations, while the effect of stream
480 velocity was of minor importance (-8%). Compared to CH₄ and CO₂, N₂O concentrations in stream and river
481 waters showed similar or stronger relationships to wastewater inflows (+16%) and upstream agricultural area
482 (+32%) (Fig 5C). Overall, the best-fit SEMs explained 60, 66, and 46 % of the observed variances in CO₂, CH₄,
483 and N₂O concentrations, respectively (Table B4)



484

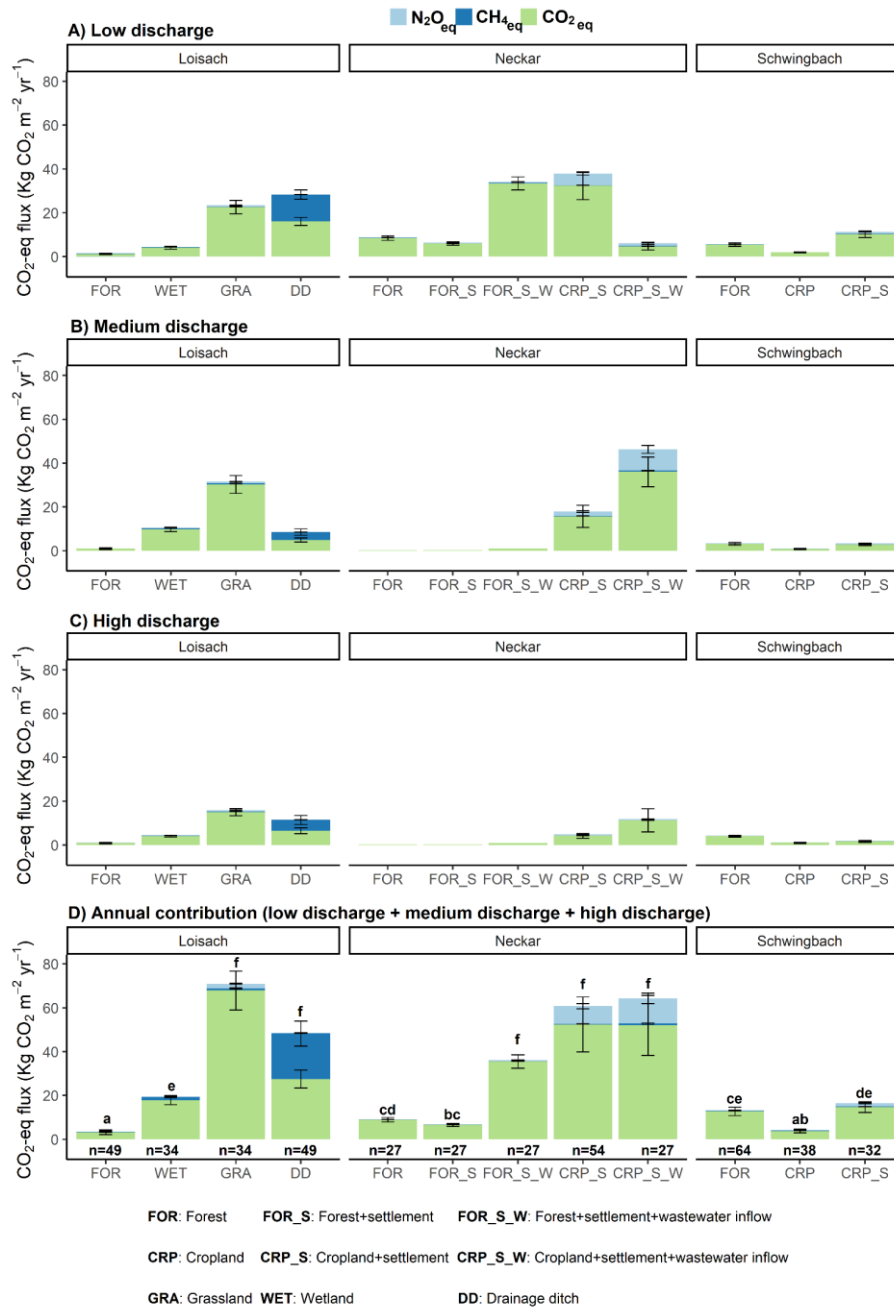
485 Fig. 5: Regression pathways predicting A) $\text{Log}_e \text{CO}_2$ concentration $\mu\text{g-C L}^{-1}$, B) $\text{Log}_e \text{CH}_4$ concentration $\mu\text{g-C L}^{-1}$ and C) $\text{Log}_e \text{N}_2\text{O}$ concentration ng-N L^{-1} across all sampling points and seasons from best-fit SEMs consisting
 486 of substrate (DO, DOC, and $\text{NO}_3\text{-N}$) and environmental variables (stream velocity (V), percentage agricultural
 487 area (AGR; grassland+cropland areas), and wastewater inflows (WW)). The numbers on the lines represent
 488 standardized slope parameters, with significant ($p\text{-value} < 0.05$) relationships indicated by *, and non-significant
 489 ($p\text{-value} > 0.05$) relationships indicated by *n.s.* Solid lines represent fitted relationships, while dashed lines
 490 represent co-variances in the environmental variables. Blue lines represent positive relationships, red represents
 491 negative relationships, with width representing the strength of the relationships.
 492

493 3.5 Annual areal fluxes

494 Based on global warming potential calculations, CO_2 dominated the annual GHG emissions across all
 495 headwater streams, with contributions ranging from 57 %–100%. The non- CO_2 gasses' contributions were much
 496 lower and ranged from 0–43% for CH_4 and 0–18% for N_2O (Fig. 6). The highest contribution of CH_4 (43%) was
 497 found at ditch sampling points in the Loisach, while the highest N_2O contributions (up to 18%) were observed at
 498 the cropland-influenced streams fed by wastewater inflows in the Neckar sub-catchments (Fig. 6). Overall, the
 499 annual CO_2 -equivalent emissions from anthropogenic-influenced streams ($\sim 71 \text{ kg CO}_2 \text{ m}^{-2} \text{ yr}^{-1}$) were up to 20

500 times higher than from natural forested streams ($\sim 3 \text{ kg CO}_2 \text{ m}^{-2} \text{ yr}^{-1}$; Fig. 6). It is also noteworthy that the total
501 annual GHG emission from oligotrophic forested streams in the Loisach catchment was significantly lower than
502 other forested catchments in the more human influenced Schwingbach and Neckar sub-catchments (Fig. 6).

503 Regarding different discharge periods, high and medium discharge periods contributed up to 91 % to
504 total GHG emissions in anthropogenic-influenced streams but only 4% in forested streams (Fig. 6). Overall, the
505 high and medium discharge periods contributed the most to the annual fluxes quantified in lower-order streams
506 (Strahler 1-2) and ditch sampling points, which were prevalent in the Loisach and Schwingbach sub-catchments
507 (Fig. 6B, C). The opposite was true for larger forested and cropland streams in the Neckar sub-catchment, where
508 higher annual flux contributions occurred primarily in the low discharge period (Fig. 6A). However, this pattern
509 did not hold for cropland streams with the wastewater inflows in the same catchment, with the sites showing an
510 82% increase in annual emissions during the high and medium discharge periods (Fig. 6 B, C).



511

512 Fig. 6: Areal CO₂-equivalent fluxes (mean ±SE) grouped by GHG type for each land use class during A) low, B)
 513 medium, and C) high discharge periods. D) represents the total annual fluxes by summing up contributions from
 514 the three discharge periods. Letters on the bar graphs represent significant differences (p<0.05) in the annual
 515 areal emissions amongst the land use classes across the three catchments based on Tukey post-hoc analyses from
 516 the linear mixed-effects models' results (Table 2)

517 4 Discussion

518 The GHG fluxes quantified from headwater streams and ditches in this study add to the growing
519 evidence that both aquatic ecosystems are significant net emitters of GHGs to the atmosphere. In agreement with
520 previous studies, CO₂ accounted for most (>81 %) of the annual fluvial GHG fluxes in CO₂ equivalents (e.g.,
521 Marescaux et al., 2018; Mwanake et al., 2022; Li et al., 2021). However, the presence of upstream agricultural
522 and settlement areas seemed to alter these trends by reducing the contribution of CO₂ and increasing N₂O and
523 CH₄ contributions. The effects of the above anthropogenic activities on aquatic GHG dynamics were twofold.
524 Drainage ditches were landscape hotspots for CH₄ emissions, while increasing upstream agricultural and
525 settlement areas resulted in fluvial N₂O hotspots. The emissions from human-influenced streams were further
526 supplemented by wastewater inflows, which provided year-long nutrients, labile carbon, and GHGs supplies,
527 resulting in much higher CO₂ and N₂O annual emissions. Besides influencing GHG hotspots, the temporal
528 dynamics of GHG fluxes from streams and ditches in our study were further impacted by anthropogenic
529 influences. While catchments dominated by wetlands or forested areas exhibited low seasonal variabilities due to
530 limitations in conditions that favor peak emissions (increased gas transfer velocities and sufficient GHG
531 supplies), opposite trends were found at catchments dominated by agricultural and settlement areas or affected
532 by wastewater inflow. These findings suggested that the occasional peak GHG emissions in the later catchments
533 represented periods where external GHG sources from supersaturated terrestrial soils or wastewater inflows
534 outweighed supply constraints during peak discharge periods with high gas transfer velocities. These findings
535 suggest that future land use changes from natural forests to agricultural and settlement areas may increase the
536 radiative forcing of aquatic GHG emissions by increasing the magnitudes of their annual fluxes, especially in a
537 changing climate with more extreme discharge conditions.

538 4.1 Seasonal variability in GHG concentrations and fluxes

539 Seasonal trends in *in situ* GHG concentrations and fluxes were mainly linked to substrate availability (C
540 and N), discharge, and temperature, similar to previous studies on other streams in temperate climates (Dismore
541 et al., 2013; Deirmendjian et al., 2019; Herreid et al., 2021). The low *in situ* CO₂ concentrations (< 100%
542 saturation) during summer (Table B2) suggested elevated photosynthetic uptake within the streams and ditches,
543 which is in line with the results of a recent meta-analysis on lotic ecosystems (Gómez-Gener et al., 2021). The
544 decline in CO₂ concentrations in summer was most apparent at the non-forested stream sampling points, with
545 higher canopy cover in the forested areas likely limiting *in situ* stream photosynthesis due to shading effects.
546 These non-forested sites also had higher instream dissolved inorganic nitrogen concentrations, nutrient
547 conditions previously shown to favor macrophyte photosynthetic uptake of CO₂, resulting in lower *in situ* stream
548 CO₂ concentrations (Deirmendjian et al., 2019). We also found that stream ditch waters were oversaturated with
549 CO₂ in autumn and winter. These seasons are characterized on the one hand by low discharge and low stream
550 velocity, conditions which likely reduce degassing rates, and on the other hand by elevated *in situ* C metabolism,
551 as supported by low DO concentration in autumn, which indicates respiratory O₂ consumption (e.g., Borges et
552 al., 2018). We attribute the lack of seasonality in CO₂ fluxes (Table B2) to the compensatory effects of
553 seasonally varying stream velocities and CO₂ source strengths. For example, high CO₂ concentrations and low

554 gas transfer velocities in autumn and vice versa in spring resulted in comparable CO₂ fluxes in the two seasons
555 (Table B2).

556 N₂O concentrations also varied significantly across seasons, but the pattern differed from that of CO₂. In
557 autumn, forested lower-order streams in the Loisach and Schwingbach catchments mainly showed N₂O
558 concentrations below atmospheric background concentrations and were temporary sinks of N₂O (Fig. 3). This
559 finding could be related to increased inputs of organic matter in these headwater catchments due to leaf fall,
560 providing additional organic carbon for microbial metabolism in this period, which likely increased the demand
561 for terminal electron acceptors such as O₂, NO₃, as well as N₂O. This conclusion is also supported by the lowest
562 DO and NO₃-N concentrations during autumn, which could suggest the dominance of complete denitrification in
563 the streams (Quick et al., 2019). With decreasing temperatures towards winter, lower productivity and N demand
564 within the streams resulted in the accumulation of NO₃-N, which seemed to favor internal N₂O production, as
565 seen by the positive relationship between the two variables (Fig. 5C). The high sensitivity of the N₂O reductase
566 to low temperatures might have further supported elevated N₂O concentration and fluxes during winter (e.g.,
567 Holtan-Hartwig et al., 2002). A similar finding of high winter N₂O concentrations and fluxes was also found in
568 other temperate streams, alluding to similar controls of temperature and nutrient availability (Herreid et al.,
569 2021; Galantini et al., 2021). Thus, based on our results, winter periods can significantly contribute to annual
570 N₂O emission budgets. Yet, to the best of our knowledge, temperate studies covering the winter period are still
571 scarce. In contrast to CO₂ and N₂O, neither CH₄ concentrations nor fluxes showed any seasonal trends. Such a
572 finding is similar to what was found in a global meta-analysis (Stanley et al., 2016), where multiple controls
573 related to substrate availability, geomorphology, and hydrology were shown to result in a high spatial-temporal
574 variance of CH₄, thus masking any seasonal emission patterns.

575 **4.2 Effect of human impacts on GHG concentrations and fluxes**

576 Anthropogenic-influenced streams and ditches draining predominantly agricultural and settlement areas
577 showed higher CO₂-equivalent GHG emissions than forested streams (Fig. 6). Such a finding is similar to other
578 studies in the temperate region (e.g., Borges et al., 2018; Deirmendjian et al., 2019; Galantini et al., 2021). The
579 high GHG emissions of streams and ditches in agricultural and settlement areas are likely due to elevated
580 hydrological inflow (e.g., via groundwater and interflow) of nitrogen and labile carbon (e.g., Lambert et al.,
581 2017; Deirmendjian et al., 2019; Mwanake et al., 2019) or terrestrially originating dissolved GHGs linked to
582 lower vegetation cover compared to forested catchments (e.g., Deirmendjian et al., 2019; Mwanake et al., 2022).
583 This interpretation could be supported by the significant positive relationships that we found between percentage
584 agriculture and stream CO₂, CH₄, and N₂O, as well as nitrate concentration and a positive trend for DOC (Figure
585 5).

586 Low DOC: DON ratios have been previously linked to more labile and less aromatic forms of dissolved
587 organic matter (DOM) (Sebestyen et al., 2008; O'Donnell et al., 2010). We found significantly lower DOC:
588 DON ratios in streams and ditches in agricultural and settlement areas than in forested streams, suggesting that
589 the more bioavailable DOM in the human-influenced ecosystems favored elevated GHGs production through
590 heterotrophic processes (e.g., Bodmer et al., 2016). Such differences in DOC: DON ratios were also found
591 amongst forested streams, with a decreasing trend from Loisach, Neckar to Schwingbach catchments, which may

592 also explain the differences in their GHG emissions (Fig. 6). The differences in the DOM bioavailability of
593 forested streams in the three catchments may suggest differences in DOM flow paths during terrestrial-
594 groundwater-stream interactions. We contend that the moderately sloping streams of the Neckar and
595 Schwingbach catchments likely had lower DOC: DON ratios due to longer water residence time and higher
596 contributions of groundwater inflow (e.g., Sebestyen et al., 2008) than those in the steeper forested catchments of
597 the Loisach (Table B3). The distinct difference in water stable isotope signatures, i.e., the shift of precipitation
598 vs. stream water seasonality across the three catchments (data not shown), further supported the difference in
599 water residence times and their relationships with stream slope (e.g., Zhou et al., 2021).

600 In addition to land use influences, wastewater inflows into streams in agricultural and settlement areas
601 further increased GHG concentrations and fluxes. The two sampled wastewater effluents, which drained into the
602 Steinlach and Ammer streams of the Neckar sub-catchments, showed higher GHG concentrations than the
603 stream water upstream of the inflows (Fig. A5, Table B1), which mainly led to increased GHG concentration and
604 fluxes also downstream of the wastewater inflows. This finding is similar to what was found in other temperate
605 studies comparing stream GHG concentration upstream and downstream of wastewater inflows (e.g., Marescaux
606 et al., 2018; Aho et al., 2022). However, due to higher background GHG fluxes in the cropland than in the
607 forested sub-catchments (Fig. 4), differences in the total GHG emissions before and after wastewater inflow
608 were more pronounced in the forested sub-catchments (Fig. 6). In addition to the pronounced differences in the
609 quality of the wastewater effluent (Table B1), this finding also shows the importance of background GHG fluxes
610 as influenced by catchment land use in assessing how wastewater inflows affect riverine GHG emissions.

611 Apart from land use influences, GHG fluxes from streams have been previously shown to decrease
612 with stream order, as dissolved GHG inputs from groundwater and terrestrial sources also reduce (e.g., Hotchkiss
613 et al., 2015; Turner et al., 2015; Mwanake et al., 2022). While our study design was not meant to explicitly
614 assess stream order influences due to limited replication across a wide range of stream orders, we did find an
615 opposite trend with stream order, similar to other studies in anthropogenic-influenced catchments (e.g., Borges et
616 al., 2018; Marescaux et al., 2018). For example, higher-order streams (stream orders > 5) in the Neckar sub-
617 catchments dominated by croplands and with wastewater influences had either higher or comparable GHG fluxes
618 than lower-order streams (stream orders < 3) in the Loisach and Schwingbach catchments. We, therefore, show a
619 potential breakdown of stream order-GHG relationships in highly human-impacted lotic ecosystems, with
620 disproportionately higher GHG emissions than in more natural ecosystems. We also show that significant
621 nutrient and labile carbon supplies to higher-order streams, which create ideal conditions for GHG production
622 and emission, may outweigh the physical disadvantages (e.g., lower surface area to volume ratio) of higher-order
623 streams relative to lower-order streams.

624 Drainage ditches, characterized by low flow velocities and high DOC: DIN ratios, functioned as strong
625 sources of CO₂ and CH₄ fluxes compared to streams. In addition to draining CO₂ and CH₄-rich wetland and
626 grassland soils, we assume that the low DO, high DOC, and low NO₃-N concentrations, along with high water
627 retention times, supported high *in situ* CH₄ production rates in the ditch sediments, resulting in their overall
628 highest contribution of CH₄ fluxes to total annual GHG emission budgets than streams (Figure 6). This
629 interpretation is further supported by a significant negative relationship between CH₄ and DO, as well as NO₃-N
630 concentrations, and a positive relationship with DOC concentrations, associations which have also been
631 previously linked to *in situ* methane production in fluvial ecosystems (e.g., Baulch et al., 2011b; Schade et al.,

632 2016). High CH₄ fluxes from drainage ditches were also found in other studies from both forested and wetland
633 areas (e.g., Schrier-Uijl et al., 2011; Peacock et al., 2021b). Contrastingly, ditches were only weak sources or
634 even sinks for atmospheric N₂O. This finding suggests N₂O reduction to N₂ via complete denitrification, an
635 interpretation already made in previous studies on lotic ecosystems (e.g., Baulch et al., 2011; Mwanake et al.,
636 2019).

637 **4.3 Comparison of GHG flux magnitudes with regional and global studies**

638 This study's daily CH₄ and N₂O diffusive flux ranges from both streams and ditches are mostly within
639 the same order of magnitude as those previously reported in global synthesis studies (Table 3: Hu et al., 2016;
640 Stanley et al., 2016). In contrast, this study reported among the highest fluvial CO₂ emissions compared to other
641 regional and global studies, with significant mean fluxes of up to 51 g-C m⁻² d⁻¹ (Table 3). We attribute this
642 finding to moderate-steep slopes such as those quantified in the mountain streams of the Loisach catchment or
643 diffuse and point terrestrial dissolved CO₂ inputs from the more human-influenced Schwingbach and Neckar
644 catchments, translating to higher fluvial CO₂ fluxes (Fig. 6). However, our high CO₂ fluxes are comparable with
645 those quantified from other temperate streams in Canada and Switzerland with similar moderate-steep slopes and
646 considerable dissolved CO₂ inputs from terrestrial landscapes (e.g., McDowell & Johnson, 2018; Horgby et al.,
647 2019). The CH₄ fluxes from streams in this study are comparable with those previously found in temperate sub-
648 catchments with similar land uses and altitudes but are lower than those reported from permafrost streams in
649 China (Table 3; Zhang et al., 2020). Our N₂O fluxes from cropland, settlement, and wastewater-influenced
650 streams are higher than those previously reported in a mixed land use catchment (Schade et al., 2016). Still, our
651 forest N₂O fluxes are in the same range as those of other temperate forested streams (Aho et al., 2022). That said,
652 these comparisons may be hampered, particularly for fluvial N₂O fluxes, by the limited number of available
653 studies (Table 3).

654 The average ditch CH₄ fluxes in this study are higher than those reported for forest and wetland draining
655 ditches in boreal and temperate regions (Table 3: Schrier-Uijl et al., 2011, Peacock et al., 2021a) and the global
656 mean provided by Peacock et al., (2021), which includes estimates from large canals. In contrast, N₂O fluxes

Table 3: Compilation of GHG emissions from temperate streams and ditches with comparable land use, climate, and altitude ranges.

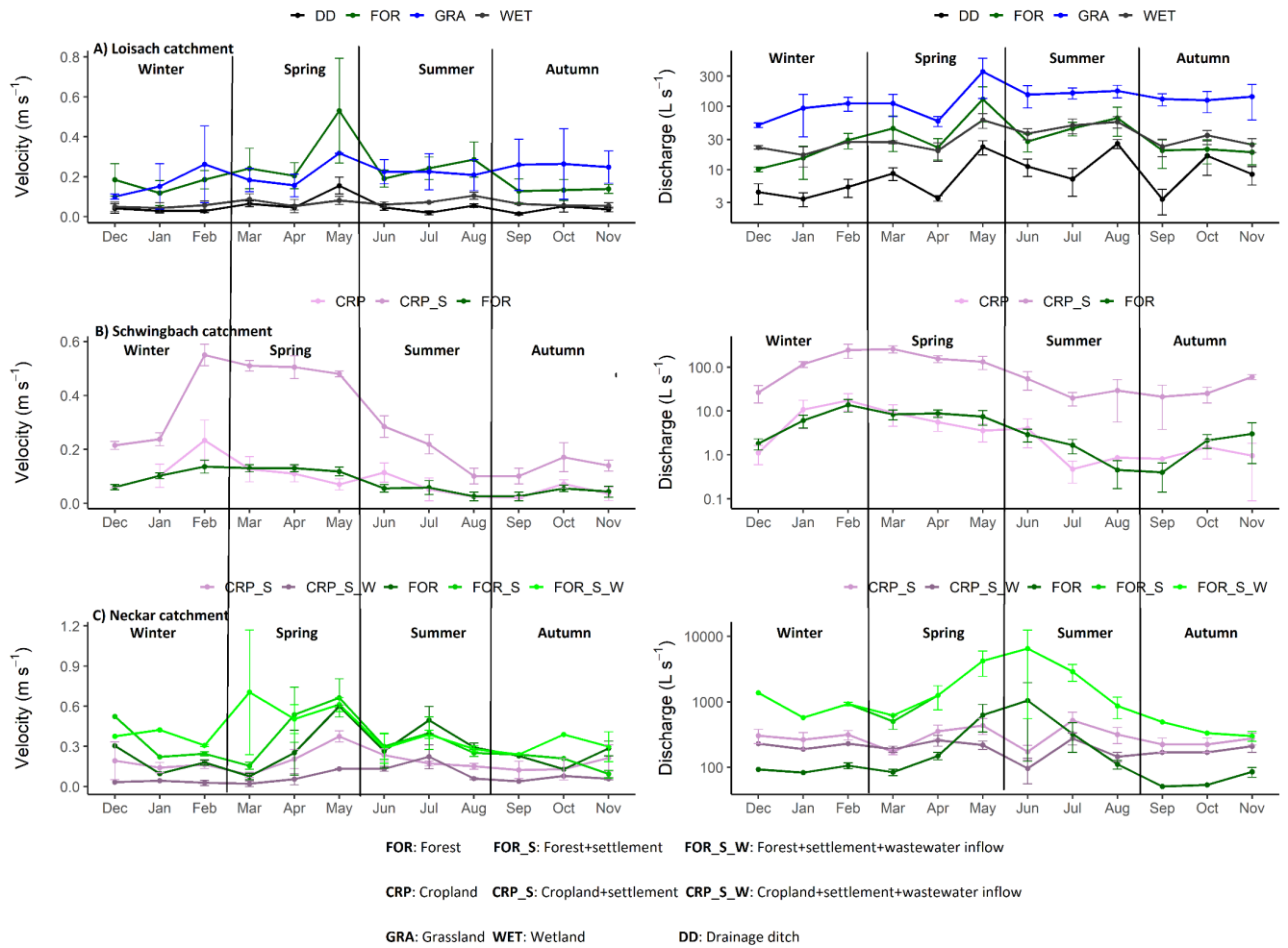
657 from ditches in this study are lower than those quantified from NO₃-N-rich agricultural ditches in temperate
 658 regions (Table 3: Reay et al., 2003).
 659

Land use/land cover	Climate	Country	Geographical coordinates (Altitude (m) reaches)	Number of study reaches	Number of observations	CO ₂ -C flux (g m ⁻² d ⁻¹)			CH ₄ -C flux (mg m ⁻² d ⁻¹)			N ₂ O-N flux (mg m ⁻² d ⁻¹)			Reference
						Range	Mean	Standard deviation	Range	Mean	Standard deviation	Range	Mean	Standard deviation	
Forest/Loisach streams	Temperate	Germany	Table 1 616–2963	3	51	-0.05	-17.4	2.4	-0.4	-164	10.5	-9.2	-20.3	1.1	This study
Forest/Schwabach streams	Temperate	Germany	Table 1 176–480	5	27	0.08	-33.4	9.5	-0.02	-54.6	9.9	-1.6	-9.6	2.1	This study
Forest/Neckar rivers	Temperate	Germany	Table 1 319–610	1	80	0.6	-14.7	6.6	0.6	-28.9	9.1	-6.9	-5.9	0.3	This study
Forest/settlement/Neckar rivers	Temperate	Germany	Table 1 319–610	1	27	0.6	-14.9	4.9	0.4	-17.3	3.9	-7.7	-6.0	2.2	This study
Forest/settlement/wastewater/Neckar rivers	Temperate	Germany	Table 1 319–610	1	27	12	-71.7	28.3	1.4	-15.2	6.5	-2.8	-17.1	3.9	This study
Wetland/Loisach streams	Temperate	Germany	Table 1 616–2963	2	34	2.8	-25.2	13.3	17.2	-237.5	101.7	-1.6	-2.9	0.8	This study
Grassland/Loisach streams	Temperate	Germany	Table 1 616–2963	2	34	6.1	-115.9	50.7	1.3	-324.5	73.2	-0.8	-25.5	12.4	This study
Cropland/Schwabach streams	Temperate	Germany	Table 1 176–480	3	48	0.3	-9.0	2.1	0.07	-5.6	0.9	-0.8	-1.8	1.9	This study
Cropland/settlement/Schwabach streams	Temperate	Germany	Table 1 176–480	2	32	0.6	-32.0	8.6	0.6	-52.6	14.9	-0.8	-22.4	6.5	This study
Cropland/settlement/Neckar rivers	Temperate	Germany	Table 1 319–610	2	54	4.5	-181.3	39.1	1.6	-77.5	21	8.4	-165.7	46.9	This study
Cropland/settlement-wastewater/Neckar rivers	Temperate	Germany	Table 1 319–610	1	27	1.1	-129.9	38.8	0.8	-301.9	58.2	6.3	-198.2	67.6	This study
Forest streams	Temperate	USA	43.0760° N, 107.2905° W	1211–3311	1	253	1.5	-6.79	1.3	14.4	-576	28.8			Kuhn et al., 2017
Forest streams	Temperate	USA	40.2140° N, 105.4332° W	2780–3505	2	11	0.2	-1.6	0.49	0.3	-7.8	2.1			Crawford et al., 2015
Forest streams	Temperate	USA	41.6032° N, 73.0877° W	270–810	7	608									Abo et al., 2022
Forest streams	Temperate	USA	41.6032° N, 73.0877° W	270–810	7	608									Abo et al., 2021
Forest streams	Temperate	Canada	49.270° N, 122.560° W	1200–3050	1	37	-1.2	-152	3.4	0.3	-2870	28.7			McDowell and Johnson, 2018
Mixed streams	Temperate	USA	43.123° N, 71.1219° W	165–348	3	37	8.7	-1980	55.9						Schade et al., 2016
Mixed streams	Temperate	Switzerland	46.1512° N, 7.0634° E	1190–3051	1	300	13.3	-494.5	31	6	-43.8				Hogbly et al., 2019
Mixed streams	Temperate	Europe	33.0000° N, 88.0000° E	1659–4600	4	107	-0.8	-5.8		0.5	-8820				Attermeier et al., 2021
Wetland streams	Subtropical	China			34	17									Zhang et al., 2020
	Global														Li et al., 2021
	Global														Hu et al., 2016
	Global														Staley et al., 2016
Drainage ditches	Global														Penczek et al., 2021
Grassland drainage ditches	Temperate	Sweden	Table 1 616–2963	3	64	2	-63.3	13.7	0.2	-793	130				This study
Forest drainage ditches	Hemiboreal	Sweden	59.5129° N, 17.3841° E	21–65	109	0.2	-3.3		116.6	-7933	1532				Penczek et al., 2021a
Wetland drainage ditches	Temperate	Netherlands	52.2200° N, 4.5300° E	1–10	7				0.2	-53					Schrier-Uijt et al., 2011
Agricultural drainage ditches	Temperate	Scotland	65.5000° N, 3.2400° W	-58–68	10	22									Reay et al., 2003

661 Conclusions

662 Streams and ditches in agricultural and settlement areas were characterized by significantly higher
663 GHG fluxes with more significant intra-annual variabilities than forests and wetlands. A combination of
664 wastewater inflows and agricultural land use resulted in the highest fluvial CO₂, CH₄, and N₂O fluxes,
665 particularly during high discharge periods with substantial external dissolved GHGs. In general, anthropogenic
666 activities resulted in a potential breakdown of the expected decrease of the GHG source strengths with increasing
667 stream order, as higher-order streams in the Neckar sub-catchments with cropland and settlement influences had
668 either higher or comparable concentrations and fluxes than small streams in the Loisach and Schwingbach
669 catchments. As most studies use stream order to upscale local and regional riverine fluxes, we show from our
670 results that caution must be taken in applying the methodology, particularly across catchments differing in land
671 use intensity.

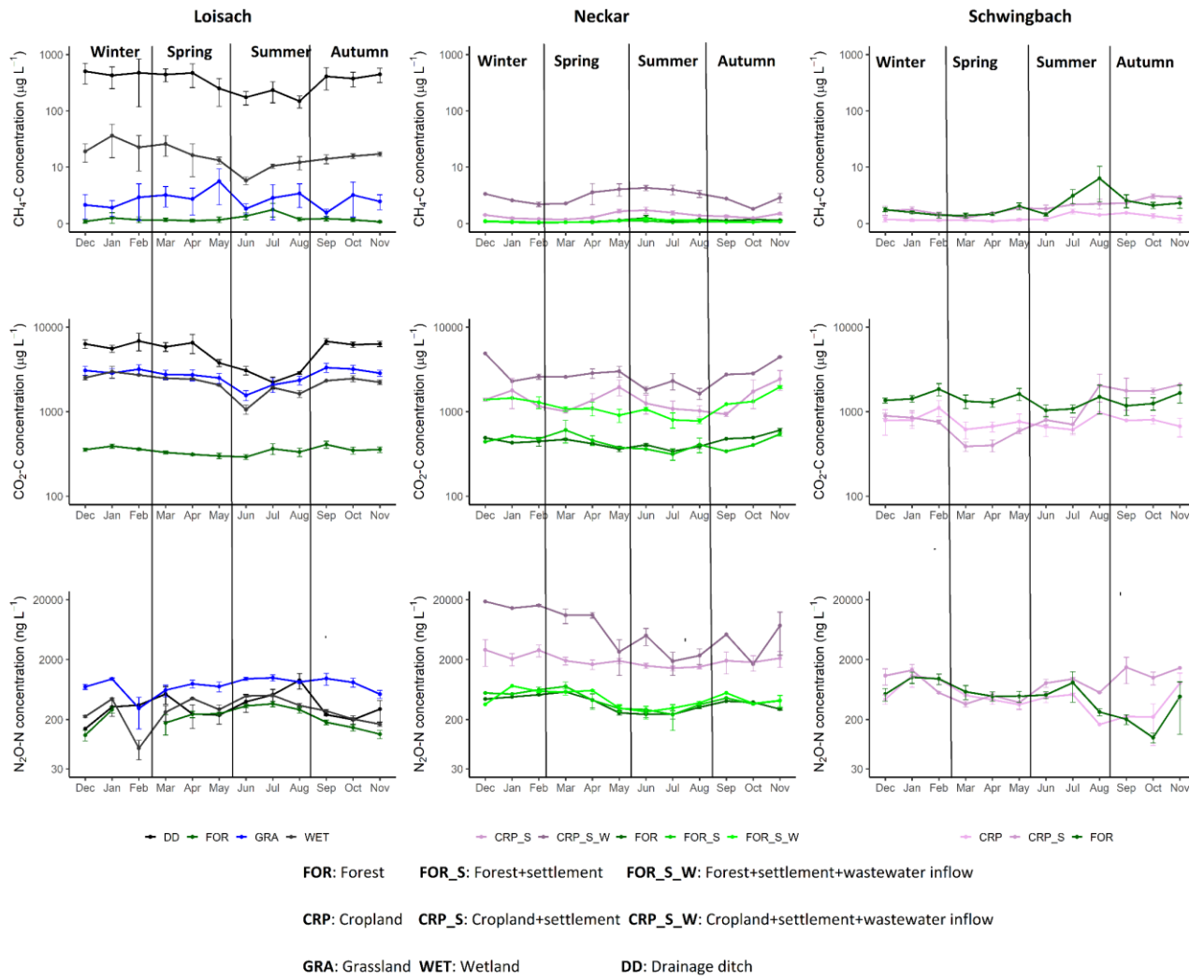
672 Our findings indicate that future work should focus more on human-influenced headwater stream
673 ecosystems, as they contribute disproportionately large annual fluxes and are more temporally variable than
674 natural ones. Our study also found higher winter N₂O fluxes, emphasizing the need for continuous sampling
675 regimes covering full years to reduce uncertainty in annual GHG emission estimates. Combining continuous
676 sampling regimes of all three biogenic GHGs (CO₂, N₂O, and CH₄) across catchments with contrasting land uses
677 will further constrict riverine emissions and aid in developing targeted emission reduction mitigation strategies..



680

681 Fig. A1: Monthly mean \pm SE velocity and discharge grouped by landuse / landcover classes in the A) Loisach,

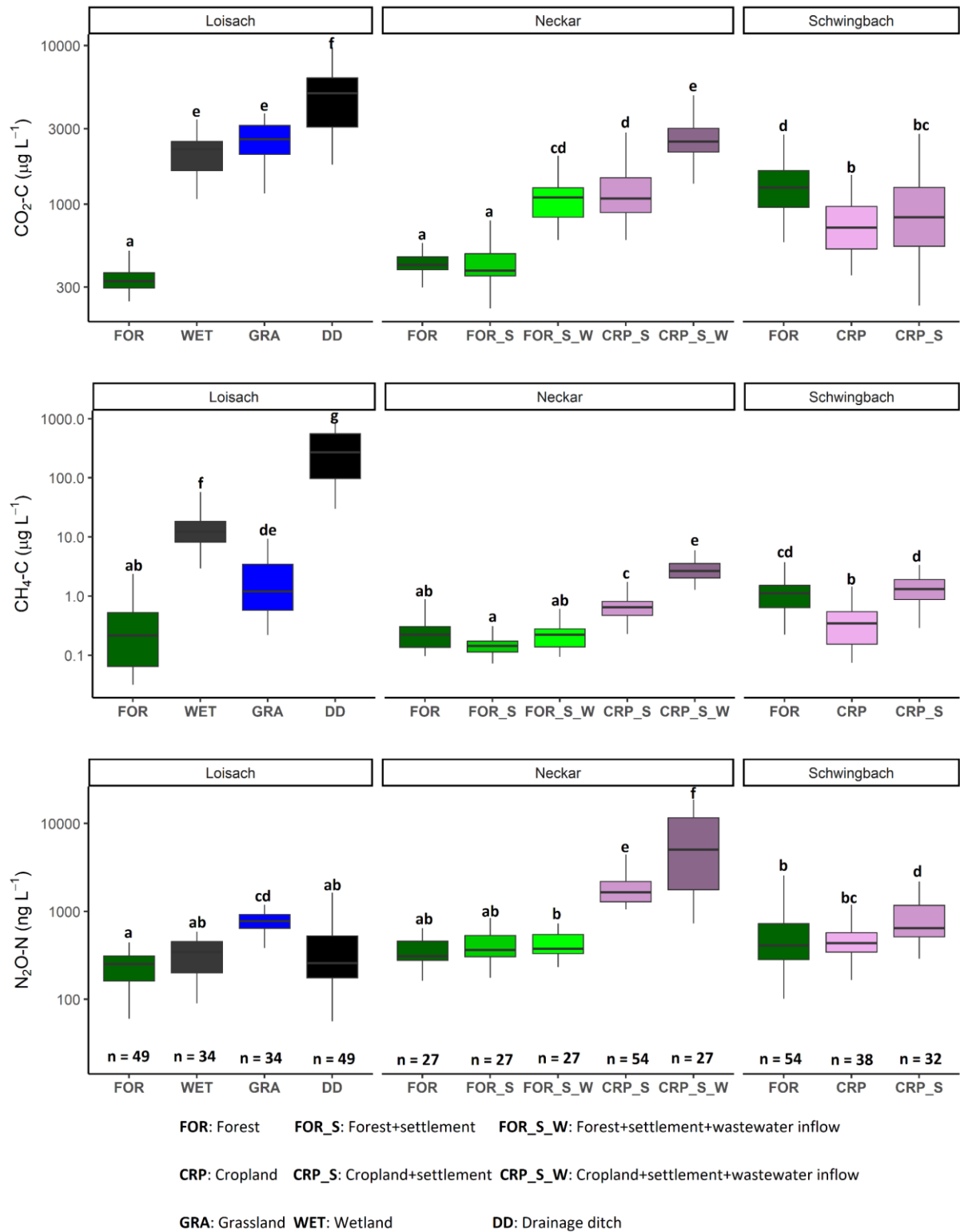
682 B) Schwingbach and C) Neckar catchments.



683

684 Fig. A2: Monthly mean ± SE CO₂, CH₄ and N₂O concentrations at sites within the Loisach, Neckar and
 685 Schwingbach catchments.

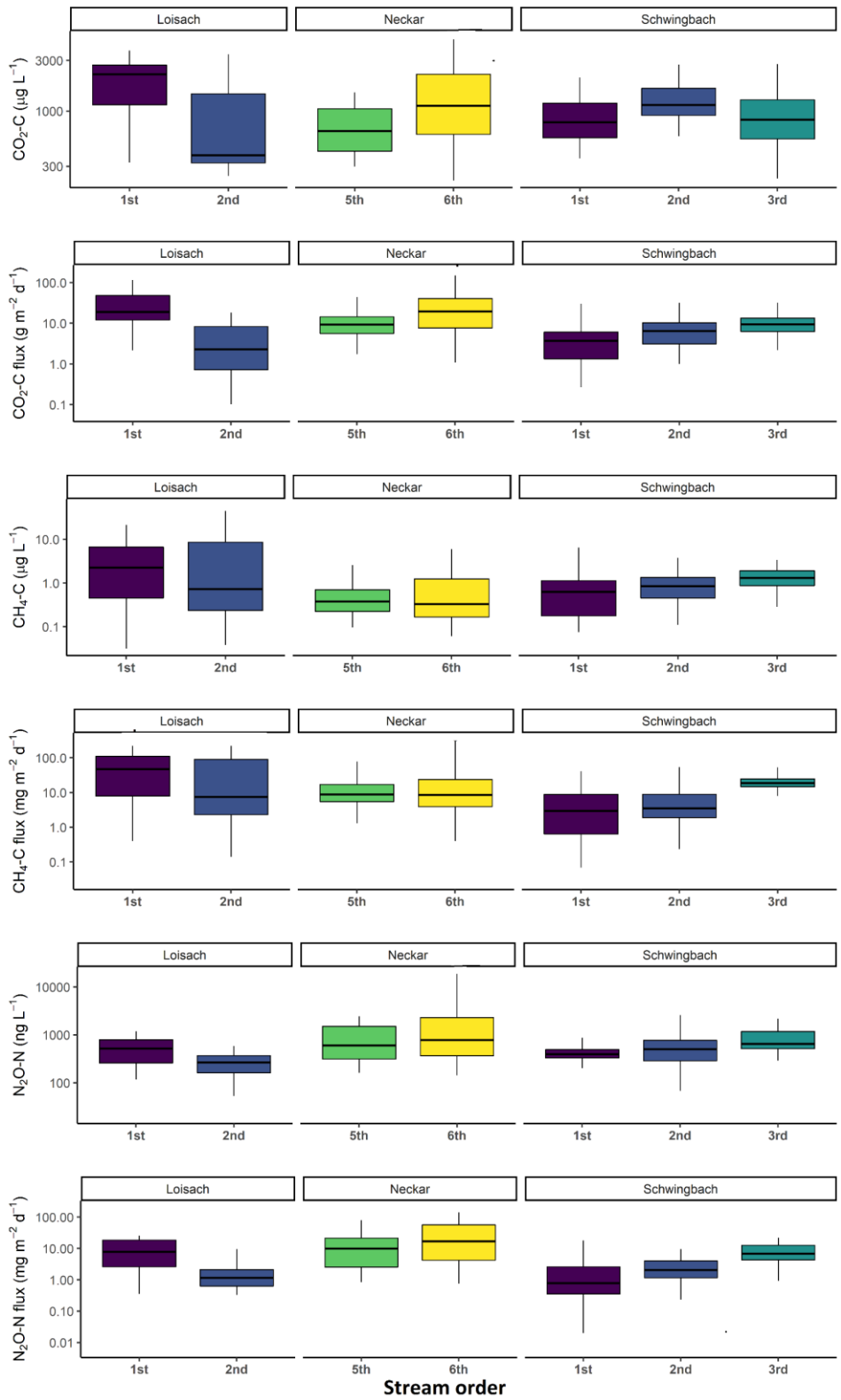
686



687

688 Fig. A3: Boxplots of CO₂, CH₄, and N₂O concentrations in stream and ditch waters in the three catchments
 689 grouped by dominating land uses (see Table 1 methods). Letters on top of the boxplots represent significant
 690 differences (p<0.05) amongst the land use classes across the three catchments based on Tukey post-hoc analyses
 691 from the linear mixed-effects models' results (Table 2).

692



693

694 Fig. A4: Boxplots of stream CO_2 , CH_4 , and N_2O concentrations and fluxes in the three catchments grouped by
 695 stream order (see Table 1 methods).

S

696 **Appendix B: Tables**

697 Table B1: Annual means (+SE) of water chemistry variables and gas concentration measured in the effluents of
 698 the Ammer (WWA) and Steinlach (WWS) wastewater treatment plants.

Water quality variables and discharge	Wastewater effluent quality from inflow zones (Annual Mean \pm SE)	
	Ammer WWA	Steinlach WWS
Temperature ($^{\circ}$ C)	13.85 \pm 0.61	13.72 \pm 0.65
pH	7.58 \pm 0.07	7.37 \pm 0.09
DO (mg L ⁻¹)	6.01 \pm 0.32	5.99 \pm 0.34
Specific Conductivity	1017.96 \pm 63.08	776.68 \pm 63.48
NO ₃ -N (mg L ⁻¹)	7.57 \pm 0.6	6.33 \pm 0.47
NH ₄ -N (mg L ⁻¹)	0.14 \pm 0.02	0.09 \pm 0.03
DOC (mg L ⁻¹)	6.8 \pm 0.33	5.66 \pm 0.58
TDN (mg L ⁻¹)	8.43 \pm 0.88	7.58 \pm 0.88
CO ₂ -C concentration (μ g L ⁻¹)	4020.08 \pm 192.75	4529.3 \pm 224.37
CH ₄ -C concentration (μ g L ⁻¹)	2.13 \pm 0.3	0.73 \pm 0.09
N ₂ O-N concentration (ng L ⁻¹)	9255.11 \pm 1563.23	483.23 \pm 61.35

699

700 Table B2: Seasonal means (+SE) of water physico-chemical variables, gas concentration and flux measured in
 701 the Loisach, Neckar and Schwingbach catchments. Letters beside the means represent significant differences
 702 ($p < 0.05$) amongst the seasons across the three catchments based on Tukey post-hoc analyses from the linear
 703 mixed-effects models' results (Table 2).

	Summer	Autumn	Winter	Spring
Temperature ($^{\circ}$ C)	14.04 \pm 0.2 d	9.83 \pm 0.32 c	5.55 \pm 0.21 a	8.38 \pm 0.22 b
pH	7.85 \pm 0.03 a	7.88 \pm 0.04 ab	7.98 \pm 0.04 b	7.96 \pm 0.04 ab
DO (mg L^{-1})	8.71 \pm 0.18 a	8.55 \pm 0.29 a	9.63 \pm 0.27 b	9.85 \pm 0.22 b
Specific Conductivity	612.03 \pm 21.8 a	606.91 \pm 28.44 b	600.86 \pm 32.62 ab	555.63 \pm 24.03 a
NO ₃ -N (mg L^{-1})	2.54 \pm 0.22 a	2.14 \pm 0.29 a	2.86 \pm 0.28 b	2.6 \pm 0.22 ab
NH ₄ -N (mg L^{-1})	0.11 \pm 0.01 a	0.14 \pm 0.02 a	0.13 \pm 0.02 a	0.1 \pm 0.01 a
TN (mg L^{-1})	2.9 \pm 0.22 a	2.49 \pm 0.3 a	3.01 \pm 0.36 b	3 \pm 0.29 ab
DON (mg L^{-1})	0.5 \pm 0.07 a	0.75 \pm 0.15 a	1.56 \pm 0.26 a	1.3 \pm 0.24 a
DOC (mg L^{-1})	4.37 \pm 0.24 a	4.26 \pm 0.36 a	4.1 \pm 0.31 a	4.66 \pm 0.26 a
DOC:DIN	11.45 \pm 2.9 b	7.21 \pm 1.37 ab	4.14 \pm 0.75 a	7.21 \pm 1.81 b
DOC:DON	103.91 \pm 56.91 a	183.33 \pm 140.18 a	13.19 \pm 2.37 a	28.33 \pm 7.31 a
Stream velocity (m s^{-1})	0.18 \pm 0.01 ab	0.12 \pm 0.01 a	0.16 \pm 0.01 ab	0.24 \pm 0.02 b
Discharge L s^{-1}	526.41 \pm 171.4 ab	86.25 \pm 13.07 a	157.3 \pm 31.58 ab	384.08 \pm 96.29 b
CO ₂ concentration ($\mu\text{g-C L}^{-1}$)	1198.93 \pm 71.66 a	2222.22 \pm 208.63 c	1869.06 \pm 185.95 c	1666.03 \pm 148.04 b
CH ₄ concentration ($\mu\text{g-C L}^{-1}$)	20.94 \pm 5.36 a	58.08 \pm 17.8 a	46.98 \pm 18 a	40.94 \pm 13.03 a
N ₂ O concentration (ng-N L^{-1})	816.06 \pm 75.58 ab	796.45 \pm 169.08 a	1691.19 \pm 400.62 b	1021.38 \pm 185.45 ab
$k_{600} \text{ md}^{-1}$	32.31 \pm 3.09 ab	22.71 \pm 2.8 a	24.54 \pm 3.36 ab	33.92 \pm 3.42 b
CO ₂ flux ($\text{mg-C m}^{-2} \text{ d}^{-1}$)	17008.98 \pm 1876.63 a	22710.21 \pm 3422.95 a	14836.51 \pm 1835.54 a	20592.21 \pm 2563.97 a
CH ₄ flux ($\text{mg-C m}^{-2} \text{ d}^{-1}$)	121.65 \pm 30.93 a	233.99 \pm 84.4 a	157.33 \pm 73.04 a	262.87 \pm 89.31 a
N ₂ O flux ($\text{mg-N m}^{-2} \text{ d}^{-1}$)	13.69 \pm 2.22 b	9.63 \pm 2.86 a	16.12 \pm 4.05 b	10.64 \pm 2.11 ab

704

Table B3: Annual mean \pm standard errors of measured water physico-chemical variables, GHG concentration, and flux for land use classes in the Loissach (FOR: forest, WET: wetland, GRA: grassland, and DD: drainage ditches), the Neckar (FOR, FOR_S: forest+settlement, FOR_S_W: forest+settlement+wastewater inflow, CRP_S: cropland+settlement, and CRP_S_W: cropland+settlement+wastewater inflow, and the Schwingbach catchment (FOR, CRP: cropland and CRP_S). The number of observations in each land use class is represented by "n" in brackets. Letters beside the means represent significant differences ($p < 0.05$) amongst the land use classes across the three catchments based on Tukey post-hoc analyses from the linear mixed-effects models' results (Table 2).

	Loissach				Neckar				Schwingbach			
	FOR (n=49)	WET (n=34)	GRA (n=34)	DD (n=49)	FOR (n=27)	FOR_S (n=27)	FOR_S_W (n=27)	CRP_S_W (n=27)	FOR (n=64)	CRP (n=38)	CRP_S (n=32)	
Temperature ($^{\circ}$ C)	8 \pm 0.5 a	8.6 \pm 0.4 ab	9.5 \pm 0.2 bd	9 \pm 0.5 bc	10.44 \pm 1.01 bd	11.6 \pm 1.01 de	12.14 \pm 0.85 ef	13.06 \pm 0.63 f	9.7 \pm 0.5 bc	9.9 \pm 0.7 cdef	9.8 \pm 0.8 bc	
pH	8.3 \pm 0.01 de	7.7 \pm 0.01 b	7.6 \pm 0.01 b	7.3 \pm 0.01 a	8.45 \pm 0.05 e	8.44 \pm 0.05 e	8.07 \pm 0.05 cd	7.72 \pm 0.08 b	7.7 \pm 0.01 b	8 \pm 0.01 c	8 \pm 0.1 c	
DO (mg L^{-1})	11 \pm 0.1 de	8.3 \pm 0.2 c	7.4 \pm 0.2 b	4.2 \pm 0.3 a	11.49 \pm 0.39 de	11.57 \pm 0.33 de	10.62 \pm 0.31 d	8.3 \pm 0.29 bc	8.8 \pm 0.1 c	8.9 \pm 0.1 c	9 \pm 0.1 c	
Specific Conductivity	365.1 \pm 8.1 a	436.9 \pm 9.4 ab	447.7 \pm 2.3 bc	484.9 \pm 16.2 bcd	738.51 \pm 51.37 g	582.07 \pm 13.96 de	700.87 \pm 31.16 fg	971.46 \pm 41.76 h	389.7 \pm 18.8 ab	597.2 \pm 13 ef	566.4 \pm 20.2 ce	
NO ₃ -N (mg L^{-1})	0.8 \pm 0.01 cd	0.5 \pm 0.01 b	0.8 \pm 0.01 cd	0.1 \pm 0.01 a	0.57 \pm 0.04 bc	2.39 \pm 0.13 e	3.73 \pm 0.29 ef	7.18 \pm 0.38 gh	1.5 \pm 0.1 d	4.9 \pm 0.4 fg	2.3 \pm 0.2 e	
NH ₄ -N (mg L^{-1})	0.01 \pm 0.001 ab	0.01 \pm 0.001 a	0.01 \pm 0.001 a	0.3 \pm 0.001 d	0.07 \pm 0.02 bc	0.1 \pm 0.01 cd	0.11 \pm 0.02 cd	0.14 \pm 0.02 d	0.1 \pm 0.01 d	0.1 \pm 0.01 d	0.1 \pm 0.01 d	
TN (mg L^{-1})	0.7 \pm 0.01 b	0.4 \pm 0.01 a	0.7 \pm 0.01 b	0.9 \pm 0.1 b	0.73 \pm 0.06 b	2.3 \pm 0.11 cd	3.92 \pm 0.3 ef	7.24 \pm 0.53 h	2.2 \pm 0.2 c	6.1 \pm 0.5 fg	3 \pm 0.3 de	
DON (mg L^{-1})	0.08 \pm 0.02 ab	0.03 \pm 0.02 a	0.06 \pm 0.03 acd	0.45 \pm 0.04 cd	0.35 \pm 0.05 d	0.26 \pm 0.08 bd	1.02 \pm 0.33 de	3.6 \pm 1.03 e	0.65 \pm 0.11 d	1.45 \pm 0.24 ce	0.75 \pm 0.1 de	
DOC (mg L^{-1})	2.9 \pm 0.3 b	1.8 \pm 0.1 a	1.5 \pm 0.1 a	9.5 \pm 0.7 g	5.9 \pm 0.67 fg	4.22 \pm 0.35 bc	4.12 \pm 0.39 cdf	4.67 \pm 0.23 ef	4.8 \pm 0.2 ef	3.8 \pm 0.1 cde	4.7 \pm 0.2 ef	
DOC:DIN	4.23 \pm 0.46 ef	4.48 \pm 0.73 ef	2.06 \pm 0.22 d	45.14 \pm 8.27 h	13.19 \pm 2.32 g	1.84 \pm 0.24 cd	1.64 \pm 0.23 cd	0.85 \pm 0.09 ab	5.89 \pm 1.1 f	1.25 \pm 0.17 bc	2.82 \pm 0.3 de	
DOC:DON	694.26 \pm 615.24 g	861.15 \pm 610.89 h	93.39 \pm 57.03 cdf	37.84 \pm 3.02 fg	60.73 \pm 30.87 efg	46.02 \pm 16.38 dfg	18.06 \pm 10.65 acd	5.68 \pm 1.9 a	37.19 \pm 15.88 df	9.02 \pm 2.67 ac	13.13 \pm 2.9 bcde	
Stream velocity (m s^{-1})	0.22 \pm 0.03 cd	0.07 \pm 0.01 b	0.22 \pm 0.02 cd	0.05 \pm 0.01 a	0.3 \pm 0.04 de	0.34 \pm 0.04 ce	0.4 \pm 0.04 e	0.19 \pm 0.02 d	0.09 \pm 0.01 ab	0.1 \pm 0.01 ab	0.29 \pm 0.03 de	
Discharge L s^{-1}	37.7 \pm 7.3 c	34.5 \pm 3.2 cd	142.1 \pm 20.6 ef	11.1 \pm 1.4 b	290.56 \pm 109.66 efg	2053.15 \pm 705.38 g	2117.15 \pm 730.03 g	318.55 \pm 32.65 f	5.4 \pm 0.7 a	5.4 \pm 1.3 a	94 \pm 15.5 de	
CO ₂ -C concentration ($\mu\text{g L}^{-1}$)	337.9 \pm 9.1 a	2075.3 \pm 107.8 e	2559.5 \pm 123.8 e	4913.5 \pm 285.4 f	423.85 \pm 14.6 a	426.67 \pm 24.18 a	1093.04 \pm 71.11 cd	1372.92 \pm 104.52 d	1350 \pm 65.3 d	748.9 \pm 45.1 b	1018.1 \pm 117.6 bc	
CH ₄ -C concentration ($\mu\text{g L}^{-1}$)	0.4 \pm 0.1 ab	16.2 \pm 2.2 f	2.4 \pm 0.4 de	338 \pm 37 g	0.25 \pm 0.03 ab	0.15 \pm 0.01 a	0.23 \pm 0.02 ab	3.01 \pm 0.25 e	1.5 \pm 0.2 cd	0.4 \pm 0.1 b	1.5 \pm 0.1 d	
N ₂ O-N concentration (ng L^{-1})	240.9 \pm 16.3 a	323 \pm 25.1 ab	771.1 \pm 42.2 cd	431.3 \pm 64.9 ab	355.91 \pm 24.26 ab	405.94 \pm 32.61 ab	421.75 \pm 28.5 b	6600.11 \pm 1121.92 f	569 \pm 59.6 b	540 \pm 64.5 bc	864.5 \pm 89.4 d	
k ₆₀₀ md^{-1}	80.9 \pm 10.6 f	10.5 \pm 0.7 bc	31.5 \pm 3.1 df	6.5 \pm 0.6 a	52.58 \pm 5.1 f	37.66 \pm 3.56 ef	43.41 \pm 3.2 ef	19.95 \pm 2.62 cd	11.7 \pm 1.1 ac	7.1 \pm 0.9 ab	22.9 \pm 1.8 de	
CO ₂ -C flux ($\text{g m}^{-2} \text{d}^{-1}$)	2.39 \pm 0.4 a	13.33 \pm 0.9 df	50.71 \pm 5.3 g	20.52 \pm 1.9 ef	6.66 \pm 0.8 cd	4.89 \pm 0.55 bc	28.26 \pm 2.8 fg	38.81 \pm 6.5 fg	9.54 \pm 0.9 cd	2.8 \pm 0.4 ab	10.96 \pm 1.3 cde	
CH ₄ -C flux ($\text{mg m}^{-2} \text{d}^{-1}$)	10.5 \pm 4.3 ab	101.7 \pm 8.3 f	73.2 \pm 15.7 de	1532.9 \pm 244.8 g	9.09 \pm 1.5 bc	3.88 \pm 0.7 ac	6.54 \pm 0.81 bc	58.23 \pm 13.33 e	9.9 \pm 1.3 c	1.5 \pm 0.2 a	21.5 \pm 2 de	
N ₂ O-N flux ($\text{mg m}^{-2} \text{d}^{-1}$)	1.1 \pm 0.9 a	0.8 \pm 0.2 a	12.4 \pm 1.4 c	1.2 \pm 0.4 a	0.32 \pm 0.63 a	2.2 \pm 0.64 a	3.96 \pm 0.85 ab	67.59 \pm 11.34 d	2.1 \pm 0.3 a	1.9 \pm 0.6 a	8.8 \pm 1.1 bc	

Table B4: Indices highlighting the performance of the best-fit SEMs, which indicate significant interaction pathways of both direct and indirect drivers of in-situ GHG concentrations in temperate streams, rivers, and drainage ditches. The goodness of fit index (GFI), comparative fit index (CFI), Tucker Lewis index, standardized root mean square residual (SRMR), and root means squared error of approximation (RMSEA) are measures of model goodness of fit, while the parsimony fit index (PNFI) compares the best-fit model to the theoretical-model.

Greenhouse gas (GHG)	Performance indices for the best-fit SEMs						Model comparison PNFI	
	GFI	CFI	TLI	SRMR	RMSEA	r ²	Theoretical SEM	Best-fit SEM
CO ₂ concentration (µg-C L ⁻¹)	1.00	1.00	1.00	0.02	<0.01	0.60	0.13	0.22
CH ₄ concentration (µg-C L ⁻¹)	1.00	1.00	1.00	0.02	<0.01	0.66	0.13	0.22
N ₂ O concentration (ng-N L ⁻¹)	0.99	1.00	0.98	0.03	0.04	0.47	0.13	0.22

Best-fit SEM structure:-

1. Log GHG = DO + DOC + Log NO₃ + agricultural area + wastewater inflow + stream velocity
2. Log NO₃ = DO + DOC + agricultural area + wastewater inflow + stream velocity
3. DOC = agricultural area
4. DO = DOC + stream velocity

Goodness of fit assesment:- GFI, CFI and TLI: 0.90 - 0.95; Good fit and >0.95 Excellent fit
SRMR and RMSEA: 0.05 - 0.08; Good fit and <0.05 Excellent fit

Data availability

The appendixes contain monthly, seasonal and land use specific water physico-chemical and GHG data used in this research. All raw data (xlsx format) will be made available upon request to the corresponding author via email.

Author contribution

RM, RK, GG, CG, and KB designed the field experiments. RK, KB, TH, and LB provided the infrastructural funding and RM and EW did the field and laboratory work. RM did the statistical analysis, consulting with RK and GG. RM prepared the first draft manuscript, consulting with RK. All co-authors contributed to the final version.

Acknowledgments

This research was funded by the German academic exchange service (DAAD) as part of RM's doctoral studies. Infrastructure for the research was provided by the TERENO Bavarian Alps/ Pre-Alps Observatory, funded by the Helmholtz Association and the Federal Ministry of Education and Research (BMBF). The authors would like to thank the entire laboratory staff at Karlsruhe Institute of Technology, Campus Alpin, Justus Liebig University Giessen, and the University of Tübingen for providing logistical support and supporting the gas and nutrient analyses. We also acknowledge the contributions of Alisson Kolar, Paul Levin Degott, Franz Weyerer, and Raphael Boehm during the field campaigns.

Declaration of competing interest

The authors declare that they have no conflict of interest.

References

- Aho, K. S., & Raymond, P. A.: Differential response of greenhouse gas evasion to storms in forested and wetland streams. *Journal of Geophysical Research: Biogeosciences* **124**, 649–662, <https://doi.org/10.1029/2018JG004750>, 2019.
- Aho, K. S., Fair, J. H., Hosen, J. D., Kyzivat, E. D., Logozzo, L. A., Rocher-Ros, G., Weber, L. C., Yoon, B., & Raymond, P. A.: Distinct concentration-discharge dynamics in temperate streams and rivers: CO₂ exhibits chemostasis while CH₄ exhibits source limitation due to temperature control. *Limnology and Oceanography*, **66**, 3656-3666, <https://doi.org/10.1002/lno.11906>, 2021.
- Aho, K. S., Fair, J. H., Hosen, J. D., Kyzivat, E. D., Logozzo, L. A., Weber, L. C., Yoon, B., Zarnetske, J. P., & Raymond, P. A.: An intense precipitation event causes a temperate forested drainage network to shift from N₂O source to sink. *Limnology and Oceanography*, **67**, S242-S257, <https://doi.org/10.1002/lno.12006>, 2022.
- Attermeyer, K., Casas-Ruiz, J.P., Fuss, T., Pastor, A., Cauvy-Fraunié, S., Sheath, D., Nydahl, A.C., Doretto, A., Portela, A.P., Doyle, B.C. and Simov, N.: Carbon dioxide fluxes increase from day to night across European streams. *Communications Earth & Environment*, 2(1), 118. <https://doi.org/10.1038/s43247-021-00192-w>, 2021
- Allen, G. H., Pavelsky, T. M., Barefoot, E. A., Lamb, M. P., Butman, D., Tashie, A., & Gleason, C. J.: Similarity of stream width distributions across headwater systems. *Nature Communications* **9**, 610, <https://doi.org/10.1038/A41467-018-02991-w>, 2018.
- Audet, J., Bastviken, D., Bundschuh, M., Buffam, I., Feckler, A., Klemedtsson, L., Laudon, H., Löfgren, S., Natchimuthu, S., Öquist, M., Peacock, M., & Wallin, M. B.: Forest streams are important sources for nitrous oxide emissions. *Global Change Biology* **26**, 629–641, <https://doi.org/10.1111/gcb.14812>, 2019.
- Battin, T. J., Kaplan, L. A., Findlay, S., Hopkinson, C. S., Marti, E., Packman, A. I., Newbold, J. D., & Sabater, F.: Biophysical controls on organic carbon fluxes in fluvial networks. *Nature Geoscience* **1**, 95–100, <https://doi.org/10.1038/ngeo101>, 2008.
- Battin, Tom J., Ronny Lauerwald, Emily S. Bernhardt, Enrico Bertuzzo, Lluís Gómez Gener, Robert O. Hall Jr, Erin R. Hotchkiss et al.: River ecosystem metabolism and carbon biogeochemistry in a changing world. *Nature* 613, 449-459, <https://doi.org/10.1038/s41586-022-05500-8>, 2021.
- Baulch, H. M., Schiff, S. L., Maranger, R., & Dillon, P. J.: Nitrogen enrichment and the emission of nitrous oxide from streams. *Global Biogeochemical Cycles* **25**, <https://doi.org/10.1029/2011GB004047>, 2011.
- Baulch, H. M., Dillon, P. J., Maranger, R., & Schiff, S. L.: Diffusive and ebullitive transport of methane and nitrous oxide from streams: Are bubble-mediated fluxes important? *Journal of Geophysical Research: Biogeosciences* **116**, <https://doi.org/10.1029/2011JG001656>, 2011a.
- Beaulieu, J. J., Arango, C. P., & Tank, J. L.: The effects of season and agriculture on nitrous oxide production in headwater streams. *Journal of Environment Quality* **38**, 637, <https://doi.org/10.2134/jeq2008.0003>, 2009.
- Begum, M.S., Bogard, M.J., Butman, D.E., Chea, E., Kumar, S., Lu, X., Nayna, O.K., Ran, L., Richey, J.E.,

- Tareq, S.M. and Xuan, D.T.: Localized pollution impacts on greenhouse gas dynamics in three anthropogenically modified Asian river systems. *Journal of Geophysical Research: Biogeosciences*, *126*(5), 2020JG006124, <https://doi.org/10.1029/2020JG006124>, 2021.
- Bodmer, P., Heinz, M., Pusch, M., Singer, G., & Premke, K.: Carbon dynamics and their link to dissolved organic matter quality across contrasting stream ecosystems. *Science of the Total Environment* **553**, 574–586, <https://doi.org/10.1016/j.scitotenv.2016.02.095>, 2016.
- Bolleter, W. T., Bushman, C. J., & Tidwell, P. W.: Spectrophotometric determination of ammonia as indophenol. *Analytical Chemistry* **33**, 592–594, <https://doi.org/10.1021/ac60172a034>, 1961.
- Borges, A.V., Darchambeau, F., Teodoru, C.R., Marwick, T.R., Tamooh, F., Geeraert, N., Omengo, F.O., Guérin, F., Lambert, T., Morana, C. and Okuku, E.: Globally significant greenhouse-gas emissions from African inland waters. *Nature Geoscience*, *8*(8), 637-642, <https://doi.org/10.1038/ngeo2486>, 2015.
- Borges, A.V., Darchambeau, F., Lambert, T., Bouillon, S., Morana, C., Brouyère, S., Hakoun, V., Jurado, A., Tseng, H.C., Descy, J.P., & Roland, F.A.: Effects of agricultural land use on fluvial carbon dioxide, methane and nitrous oxide concentrations in a large European river, the Meuse (Belgium). *Science of the Total Environment* **610–611**, 342–355, <https://doi.org/10.1016/j.scitotenv.2017.08.047>, 2018.
- Borges, A.V., Darchambeau, F., Lambert, T., Morana, C., Allen, G.H., Tambwe, E., Toengaho Sembaito, A., Mambo, T., Nlandu Wabakhangazi, J., Descy, J.P., & Teodoru, C.R.: Variations in dissolved greenhouse gases (CO₂, CH₄, N₂O) in the Congo river network overwhelmingly driven by fluvial-wetland connectivity. *Biogeosciences* **16**, 3801–3834, <https://doi.org/10.5194/bg-16-3801-2019>, 2019.
- Crawford, J. T., Dornblaser, M. M., Stanley, E. H., Clow, D. W., & Striegl, R. G.: Source limitation of carbon gas emissions in high-elevation mountain streams and lakes. *Journal of Geophysical Research: Biogeosciences*, **120**, 952-964, <https://doi.org/10.1002/2014JG002861>, 2015.
- Deirmendjian, L., Anschutz, P., Morel, C., Mollier, A., Augusto, L., Loustau, D., Cotovicz Jr, L.C., Buquet, D., Lajaunie, K., Chaillou, G. and Voltz, B.: Importance of the vegetation-groundwater-stream continuum to understand transformation of biogenic carbon in aquatic systems—A case study based on a pine-maize comparison in a lowland sandy watershed (Landes de Gascogne, SW France). *Science of the Total Environment*, *661*, pp.613-629, <https://doi.org/10.1016/j.scitotenv.2019.01.152>, 2019.
- Dinsmore, K. J., Wallin, M. B., Johnson, M. S., Billett, M. F., Bishop, K., Pumpanen, J., & Ojala, A.: Contrasting CO₂ concentration discharge dynamics in headwater streams: A multi-catchment comparison. *Journal of Geophysical Research: Biogeosciences*, **118**, 445-461, <https://doi.org/10.1002/jgrg.20047>, 2013.
- Drake, T. W., Raymond, P. A., & Spencer, R. G.: Terrestrial carbon inputs to inland waters: A current synthesis of estimates and uncertainty. *Limnology and Oceanography Letters*, *3*(3), 132-142, <https://doi.org/10.1002/lol2.10055>, 2018.
- Galantini, L., Lapierre, J. F., & Maranger, R.: How are greenhouse gases coupled across seasons in a large temperate river with differential land use?. *Ecosystems*, **24**, 2007-2027, <https://doi.org/10.1007/A10021-021-00629-5>, 2021.

- Gomez-Gener, L., Rocher-Ros, G., Battin, T., Cohen, M.J., Dalmagro, H.J., Dinsmore, K.J., Drake, T.W., Duvert, C., Enrich-Prast, A., Horgby, Å., & Johnson, M.S.: Global carbon dioxide efflux from rivers enhanced by high nocturnal emissions. *Nature Geoscience*, **14**, 289-294, <https://doi.org/10.1038/A41561-021-00722-3>, 2021.
- Glaser, C., Schwientek, M., Junginger, T., Gilfedder, B.S., Frei, S., Werneburg, M., Zwiener, C., & Zarfl, C.: Comparison of environmental tracers including organic micropollutants as groundwater exfiltration indicators into a small river of a karstic catchment. *Hydrological Processes*, **34**, 4712-4726, <https://doi.org/10.1002/hyp.13909>, 2020.
- Gore, J. A.: Discharge measurements and streamflow analysis. In F. R. Hauer & G. A. Lamberti (Eds.), *Methods in stream ecology*. (2nd ed., chap. 3, pp. 51–77). Cambridge, MA: Academic Press, <https://doi.org/10.1016/B978-012332908-0.50005-X>, 2007.
- Intergovernmental Panel on Climate Change.: Climate change 2013—the physical science basis: Working group I contribution to the fifth assessment report of the Intergovernmental Panel on Climate Change. Cambridge: Cambridge University Press, doi:10.1017/CBO9781107415324, 2014.
- Hall Jr, R. O., & Ulseth, A. J.: Gas exchange in streams and rivers. *Wiley Interdisciplinary Reviews: Water*, 7(1), e1391, <https://doi.org/10.1002/wat2.1391>, 2020.
- Herreid, A. M., Wymore, A. S., Varner, R. K., Potter, J. D., & McDowell, W. H.: Divergent controls on stream greenhouse gas concentrations across a land-use gradient. *Ecosystems*, **24**, 1299-1316, <https://doi.org/10.1007/A10021-020-00584-7>, 2021.
- Holtan-Hartwig, L., Dörsch, P., & Bakken, L. R.: Low temperature control of soil denitrifying communities: kinetics of N₂O production and reduction. *Soil Biology and Biochemistry*, **34**, 1797-1806, [https://doi.org/10.1016/S0038-0717\(02\)00169-4](https://doi.org/10.1016/S0038-0717(02)00169-4), 2002.
- Horgby, Å., Boix Canadell, M., Ulseth, A. J., Vennemann, T. W., & Battin, T. J.: High-resolution spatial sampling identifies groundwater as driver of CO₂ dynamics in an Alpine stream network. *Journal of Geophysical Research: Biogeosciences*, **124**, 1961-1976, <https://doi.org/10.1029/2019JG005047>, 2019.
- Hotchkiss, E. R., Hall Jr, R. O., Sponseller, R. A., Butman, D., Klaminder, J., Laudon, H., Rosvall, M., & Karlsson, J.: Sources of and processes controlling CO₂ emissions change with the size of streams and rivers. *Nature Geoscience* **8**, 696–699, <https://doi.org/10.1038/ngeo2507>, 2015.
- Hu, M., Chen, D. and Dahlgren, R.A.: Modeling nitrous oxide emission from rivers: a global assessment. *Global change biology*, 22(11), 3566-3582, <https://doi.org/10.1111/gcb.13351>, 2016.
- Kuhn, C., Bettigole, C., Glick, H. B., Seegmiller, L., Oliver, C. D., & Raymond, P.: Patterns in stream greenhouse gas dynamics from mountains to plains in northcentral Wyoming. *Journal of Geophysical Research: Biogeosciences*, **122**, 2173-2190, <https://doi.org/10.1002/2017JG003906>, 2017.
- Lambert, T., Bouillon, S., Darchambeau, F., Morana, C., Roland, F. A. E., Descy, J., & Borges, A. V.: Effects of human land use on the terrestrial and aquatic sources of fluvial organic matter in a temperate river basin (The Meuse River, Belgium). *Biogeochemistry* **136**, 191–211, <https://doi.org/10.1007/A10533-017-0387-9>,

2017.

- Li, M., Peng, C., Zhang, K., Xu, L., Wang, J., Yang, Y., Li, P., Liu, Z., & He, N.: Headwater stream ecosystem: an important source of greenhouse gases to the atmosphere. *Water Research*, **190**, 116738, <https://doi.org/10.1016/j.watres.2020.116738>, 2021.
- Marescaux, A., Thieu, V., & Garnier, J.: Carbon dioxide, methane and nitrous oxide emissions from the human-impacted Seine watershed in France. *Science of the Total Environment*, **643**, 247-259, <https://doi.org/10.1016/j.scitotenv.2018.06.151>, 2018.
- McDowell, M. J., & Johnson, M. S.: Gas transfer velocities evaluated using carbon dioxide as a tracer show high streamflow to be a major driver of total CO₂ evasion flux for a headwater stream. *Journal of Geophysical Research: Biogeosciences*, **123**, 2183-2197, <https://doi.org/10.1029/2018JG004388>, 2018.
- Mwanake, R. M., Gettel, G. M., Aho, K. S., Namwaya, D. W., Masese, F. O., Butterbach-Bahl, K., & Raymond, P. A.: Land use, not stream order, controls N₂O concentration and flux in the upper Mara River basin, Kenya. *Journal of Geophysical Research: Biogeosciences* **124**, 3491–3506, <https://doi.org/10.1029/2019jg005063>, 2019.
- Mwanake, R. M., Gettel, G. M., Ishimwe, C., Wangari, E. G., Butterbach-Bahl, K., & Kiese, R.: Basin-scale estimates of greenhouse gas emissions from the Mara River, Kenya: Importance of discharge, stream size, and land use/land cover. *Limnology and Oceanography*, **67**, 1776-1793, <https://doi.org/10.1002/lno.12166>, 2022.
- O'Donnell, J. A., Aiken, G. R., Kane, E. S., & Jones, J. B.: Source water controls on the character and origin of dissolved organic matter in streams of the Yukon River basin, Alaska. *Journal of Geophysical Research: Biogeosciences*, **115**, <https://doi.org/10.1029/2009JG001153>, 2010.
- Park, J.H., Nayna, O.K., Begum, M.S., Chea, E., Hartmann, J., Keil, R.G., Kumar, S., Lu, X., Ran, L., Richey, J.E. and Sarma, V.V.: Reviews and syntheses: Anthropogenic perturbations to carbon fluxes in Asian river systems—concepts, emerging trends, and research challenges. *Biogeosciences*, **15**(9), 3049-3069, <https://doi.org/10.5194/bg-15-3049-2018>, 2018.
- Patton, C. J., & Kryskalla, J. R.: Colorimetric determination of nitrate plus nitrite in water by enzymatic reduction, automated discrete analyzer methods. *US Geological Survey Techniques and Methods, Book 5* **34**, <https://doi.org/10.3133/tm5B8>, 2011.
- Peacock, M., Audet, J., Bastviken, D., Futter, M.N., Gauci, V., Grinham, A., Harrison, J.A., Kent, M.S., Kosten, S., Lovelock, C.E., & Veraart, A.J.: Global importance of methane emissions from drainage ditches and canals. *Environmental Research Letters*, **16**, 044010, <https://doi.org/10.1088/1748-9326/abeb36>, 2021.
- Peacock, M., Granath, G., Wallin, M. B., Högbom, L., & Futter, M. N.: Significant Emissions From Forest Drainage Ditches—An Unaccounted Term in Anthropogenic Greenhouse Gas Inventories?. *Journal of Geophysical Research: Biogeosciences*, **126**, <https://doi.org/10.1029/2021JG006478>, 2021a.
- Quick, A. M., Reeder, W. J., Farrell, T. B., Tonina, D., Feris, K. P., & Benner, S. G.: Nitrous oxide from streams and rivers: A review of primary biogeochemical pathways and environmental variables. *Earth-science*

- reviews*, 191, 224–262, <https://doi.org/10.1016/j.earscirev.2019.02.021>, 2019.
- Raymond, P.A., Zappa, C.J., Butman, D., Bott, T.L., Potter, J., Mulholland, P., Laursen, A.E., McDowell, W.H. & Newbold, D.: Scaling the gas transfer velocity and hydraulic geometry in streams and small rivers. *Limnology and Oceanography* **2**, 41–53, <https://doi.org/10.1215/21573689-1597669>, 2012.
- Reay, D. S., Smith, K. A., & Edwards, A. C.: Nitrous oxide emission from agricultural drainage waters. *Global Change Biology*, **9**, 195–203, <https://doi.org/10.1046/j.1365-2486.2003.00584.x>, 2003.
- Rocher-Ros, G., Sponseller, R. A., Lidberg, W., Mörth, C. M., & Giesler, R.: Landscape process domains drive patterns of CO₂ evasion from river networks. *Limnology and Oceanography Letters*, **4**, 87–95, <https://doi.org/10.1002/lol2.10108>, 2019.
- Schade, J. D., Bailio, J., & McDowell, W. H.: Greenhouse gas flux from headwater streams in New Hampshire, USA: Patterns and drivers. *Limnology and Oceanography* **61**, 165–17, <https://doi.org/10.1002/lno.10337>, 2016.
- Schrier-Uijl, A. P., Veraart, A. J., Leffelaar, P. A., Berendse, F., & Veenendaal, E. M.: Release of CO₂ and CH₄ from lakes and drainage ditches in temperate wetlands. *Biogeochemistry*, **102**, 265–279, <https://doi.org/10.1007/A10533-010-9440-7>, 2011.
- Schumacker, R. E., & Lomax, R. G.: A Beginner's Guide to Structural Equation Modeling (4th Ed.). New York: Routledge. 2016.
- Sebestyen, S. D., Boyer, E. W., Shanley, J. B., Kendall, C., Doctor, D. H., Aiken, G. R., & Ohte, N.: Sources, transformations, and hydrological processes that control stream nitrate and dissolved organic matter concentrations during snowmelt in an upland forest. *Water Resources Research*, **44**, <https://doi.org/10.1029/2008WR006983>, 2008.
- Shelley, F., Grey, J., & Trimmer, M.: Widespread methanotrophic primary production in lowland chalk rivers. *Proceedings of the Royal Society B: Biological Sciences*, **281** (1783), <https://doi.org/10.1098/rspb.2013.2854mWAN>, 2014.
- Stanley, E. H, Casson, N. J., Christel, S. T., Crawford, J. T., Loken, L. C., & Oliver, S. K.: The ecology of methane in streams and rivers: patterns, controls, and global significance. *Ecological Monographs* **86**, 146–171, <https://doi.org/10.1890/15-1027>, 2016.
- Strahler, A. N.: Hypsometric (area-altitude) analysis of erosional topography. *GSA Bulletin* **63**, 1117–1142, [https://doi.org/10.1130/0016-7606\(1952\)63\[1117:HAAOET\]2.0.CO;2](https://doi.org/10.1130/0016-7606(1952)63[1117:HAAOET]2.0.CO;2), 1952.
- Turner, P. A., Griffis, T. J., Lee, X., Baker, J. M., Venterea, R. T., & Wood, J. D.: Indirect nitrous oxide emissions from streams within the US Corn Belt scale with stream order. *Proceedings of the National Academy of Sciences* **112**, 9839–9843, <https://doi.org/10.1073/pnas.1503598112>, 2015.
- Wallin, M. B., Audet, J., Peacock, M., Sahlée, E., & Winterdahl, M.: Carbon dioxide dynamics in an agricultural headwater stream driven by hydrology and primary production. *Biogeosciences* **17**, 2487–2498, <https://doi.org/10.5194/bg-17-2487-2020>, 2020.

- Wallin, M.B., Campeau, A., Audet, J., Bastviken, D., Bishop, K., Kokic, J., Laudon, H., Lundin, E., Löfgren, S., Natchimuthu, S. and Sobek, S.: Carbon dioxide and methane emissions of Swedish low-order streams—A national estimate and lessons learnt from more than a decade of observations. *Limnology and Oceanography* **3**, 156–167, <https://doi.org/10.1002/lol2.10061>, 2018.
- Wang, D.; Ye, W., Wu, G., Li, R., Guan, Y., Zhang, W., Wang, J., Shan, Y., Hubacek, K.: Greenhouse gas emissions from municipal wastewater treatment facilities in China from 2006 to 2019. *Sci Data* **9**, 317, <https://doi.org/10.1038/s41597-022-01439-7>, 2022.
- Wangari, E.G., Mwanake, R.M., Kraus, D., Werner, C., Gettel, G.M., Kiese, R., Breuer, L., Butterbach-Bahl, K. and Houska, T.: Number of chamber measurement locations for accurate quantification of landscape-scale greenhouse gas fluxes: Importance of land use, seasonality, and greenhouse gas type. *Journal of Geophysical Research: Biogeosciences*, **127**, <https://doi.org/10.1029/2022JG006901>, 2022.
- Winkler, K., Fuchs, R., Rounsevell, M., & Herold, M.: Global land use changes are four times greater than previously estimated. *Nature communications*, **12**, 1-10, <https://doi.org/10.1038/A41467-021-22702-2>, 2021.
- Zhang, L., Xia, X., Liu, S., Zhang, S., Li, S., Wang, J., Wang, G., Gao, H., Zhang, Z., Wang, Q. and Wen, W.: Significant methane ebullition from alpine permafrost rivers on the East Qinghai–Tibet Plateau. *Nature Geoscience*, **13**, 349-354, <https://doi.org/10.1038/A41561-020-0571-8>, 2020.
- Zhang, W., Li, H., Xiao, Q., & Li, X.: Urban rivers are hotspots of riverine greenhouse gas (N₂O, CH₄, CO₂) emissions in the mixed-landscape chaohu lake basin. *Water Research*, **189**, 116624, <https://doi.org/10.1016/j.watres.2020.116624>, 2021.
- Zhou, J., Liu, G., Meng, Y., Xia, C., Chen, K., & Chen, Y.: Using stable isotopes as tracer to investigate hydrological condition and estimate water residence time in a plain region, Chengdu, China. *Scientific reports*, **11**, 1-12, <https://doi.org/10.1038/s41598-021-82349-3>, 2021.